



1 **Comparing Secondary Organic Aerosols Schemes Implemented in Current**  
2 **Chemical Transport Models and the Policy Implications of Uncertainties**

3 Ling Huang<sup>1</sup>, Benjie Chen<sup>1</sup>, Zi'ang Wu<sup>1</sup>, Katie Tuite<sup>2</sup>, Pradeepa Vennam<sup>2</sup>, Greg  
4 Yarwood<sup>2,\*</sup>, Li Li<sup>1,\*</sup>

5 <sup>1</sup>School of Environmental and Chemical Engineering, Shanghai University, Shanghai,  
6 200444, China

7 <sup>2</sup>Ramboll, Novato, California, 94945, USA

8 *Correspondence to:* Greg Yarwood ([gyarwood@ramboll.com](mailto:gyarwood@ramboll.com)), Li Li ([lily@shu.edu.cn](mailto:lily@shu.edu.cn))

9 **Abstract**

10 Secondary organic aerosol (SOA) constitutes a major component of fine particulate  
11 matter (PM<sub>2.5</sub>) that models must account for to assess how human activities influence  
12 air quality, climate, and public health. We characterize the current state of SOA  
13 modeling by analyzing eight SOA schemes implemented in five widely used air quality  
14 models: CAMx, CMAQ, GEOS-Chem, WRF-Chem and CHIMERE. We performed  
15 offline calculations to compare initial SOA yields, the effects of SOA aging processes,  
16 and the influence of NO<sub>x</sub> conditions on yields. Our objective is to understand variation  
17 rather than to identify a superior scheme. We find significant discrepancies in initial  
18 SOA yields leading to different precursor rankings of SOA-forming potential. The ratio  
19 of maximum to minimum initial yield spans from 1.8 to over 1000, depending upon  
20 precursor, with the median of 4.2 underscoring large uncertainties. The impact of  
21 nitrogen oxide (NO<sub>x</sub>) conditions on SOA yields is also highly variable among schemes.  
22 While some schemes include SOA aging, their treatments differ substantially, with  
23 some schemes showing large increases in SOA mass, while others exhibit minimal  
24 changes. The substantial differences among current SOA schemes highlight a lack of  
25 consensus within the air quality modelling community. Evaluating model simulation  
26 results using ambient measurements is unlikely to resolve these discrepancies because  
27 uncertainties in SOA formation and precursor emissions are deeply intertwined. The  
28 limitations of current SOA schemes should be recognized and acknowledged because  
29 model choice can greatly influence predicted SOA concentrations and their evolution,  
30 ultimately impacting air quality forecasts, assessments, and regulatory decisions.



**Keywords:** Secondary organic aerosol (SOA), chemical transport model (CTM), two-product, volatility basis set (VBS), SOA yields, CAMx, CMAQ, GEOS-Chem, WRF-Chem, CHIMERE

## 1. Introduction

Organic Aerosol (OA) contributes a large fraction of fine particulate matter (PM<sub>2.5</sub>) due to primary OA emissions (POA) and the formation of secondary OA (SOA) from anthropogenic, biogenic, and biomass burning sources (Donahue et al., 2006; Huang et al., 2014; Tsimpidi et al., 2016). SOA precursor emissions include traditional volatile organic compounds (VOC) as well as non-traditional intermediate and semi-volatile VOC (IVOC and SVOC, respectively) whereas POA are directly emitted from combustion sources. Recent studies report that volatile chemical products (VCPs) are increasingly important contributors to SOA formation (Pennington et al., 2021; Sasidharan et al., 2023). Chemical transport models (CTMs) are essential tools for understanding the sources and transport of OA as well as assessing the effectiveness of mitigation strategies (e.g. Pye et al., 2021; Chang et al., 2022; Chen et al., 2024; Pennington et al., 2024; Vitali et al., 2024). However, accurately modeling SOA formation in CTMs has posed persistent challenges due to the intricate nature of SOA formation processes (Li et al., 2023). Scientific understanding of SOA formation pathways is continuously evolving. Therefore, it is crucial to review the state of science on SOA formation implemented in different CTMs and identify existing knowledge gaps.

In general, CTMs adopt one of two approaches for SOA simulation: the two-product scheme (Figure 1) or the volatility basis set (VBS) scheme (Figure 2a). Two-product schemes apply the absorptive gas-particle partitioning theory of Pankow (1994) using only two surrogate products to represent all of the condensable gases (CGs) formed when SOA precursors are oxidized in the gas phase by OH radical, ozone (O<sub>3</sub>), or NO<sub>3</sub> radical, e.g.:



where CG1 and CG2 have different saturation concentration (C\*);  $\alpha_1$  and  $\alpha_2$  are molar



stoichiometric yields. The  $\alpha$  and  $C^*$  values for CG1 and CG2 are fitted to SOA formation observed in chamber experiments. SOA formation depends on the total amount of OA present (Pankow, 1994) and consequently SOA formation depends on POA. POA is usually treated as non-volatile in two-product schemes (e.g., Strader et al., 1999; Schell et al., 2001) but can be treated as semi-volatile in a modified two-product scheme (e.g. Huang et al. 2024).

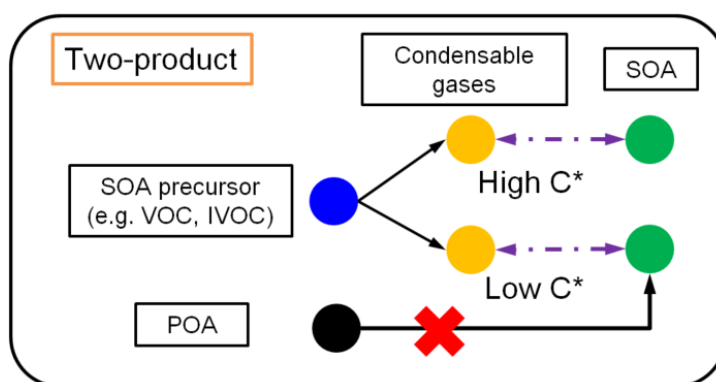
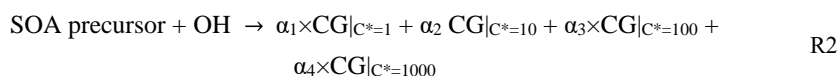


**Figure 1** Illustration of a “two-product” SOA scheme combined with a non-volatile treatment of POA

The VBS framework (Donahue et al., 2006) expands the two-product model by having more condensable gases that are systematically organized by volatility (i.e.,  $C^*$ ). Condensable organic compounds are categorized based on their volatility into bins that are typically separated by a factor of 10, e.g., four bin with  $C^*$  of 1, 10, 100, 1000  $\mu\text{g}/\text{m}^3$ :



Similar to the two-product model, the VBS framework is based on the absorptive partitioning theory and the CG yield ( $\alpha$ ) for each volatility bin can be obtained by fitting the results of laboratory studies. Many VBS schemes treat POA as being semi-volatile and able to dynamically partition between the gas and particle phase depending on environmental factors, similar to SOA. Figure 2 illustrates the “1-dimensional” (1-D) VBS framework where volatility is the dimension that varies (discretized to volatility bins) and panels a-d illustrate various treatments of SOA aging. In the 2-D VBS introduced by Donahue et al. (2011), both volatility and oxidation state can vary independently. The 1.5-D VBS introduced by Koo et al. (2014) represents variations in



81 volatility and oxidation state as a single coordinate by assuming they are related.

82 Figure 2a depicts a four-bin VBS framework with no aging of OA after the initial

83 formation of SOA. Emitted SOA precursors (e.g., VOC, IVOC) undergo initial gas-

84 phase oxidation and produce four types of CGs which can immediately condense to

85 form SOA. Beyond initial oxidation, multi-generational aging processes can occur and

86 include functionalization and/or fragmentation of gas-phase CGs, oligomerization of

87 condensed-phase SOA, SOA photolysis, and heterogeneous SOA oxidation.

88 Functionalization and oligomerization typically increase SOA mass by lowering

89 volatility, whereas fragmentation and photolysis decrease SOA mass. Figure 2b depicts

90 a VBS framework incorporating a step-wise OH-oxidation functionalization process as

91 included in many VBS schemes, where CGs undergo gas-phase reactions (usually

92 parameterized as OH-oxidation) that add oxygen-containing functional groups and

93 successively lower volatility. This functionalization increases molecular weight with

94 each oxidation generation, which can be parameterized as a percentage increase

95 (usually 7.5% or 15%) to account for added oxygen (Robinson et al., 2007; Shrivastava

96 et al., 2015). Gas-phase reactions of CGs can cause molecular fragmentation as well as

97 functionalization. As SOA ages, fragmentation reactions may gain significance (Cappa

98 et al. 2012). Figure 2c shows a VBS framework with both functionalization and

99 fragmentation. In this scheme, OH-oxidation of the CGs forms products across lower

100 (due to functionalization) and higher (due to fragmentation) volatility bins that are often

101 parameterized using predefined fractions. Particle-phase oligomerization, as illustrated

102 by Figure 2d, is another SOA aging process where condensed SOA molecules join

103 together and form larger SOA molecules with extremely low volatility. Some schemes

104 refer to oligomerization as polymerization. Typically, the rate of oligomerization is

105 modeled as independent of the gas-phase oxidant level.

106 Given the diverse treatments of SOA formation employed in CTMs, it is both necessary

107 and important to comprehensively understand and quantify the similarities and

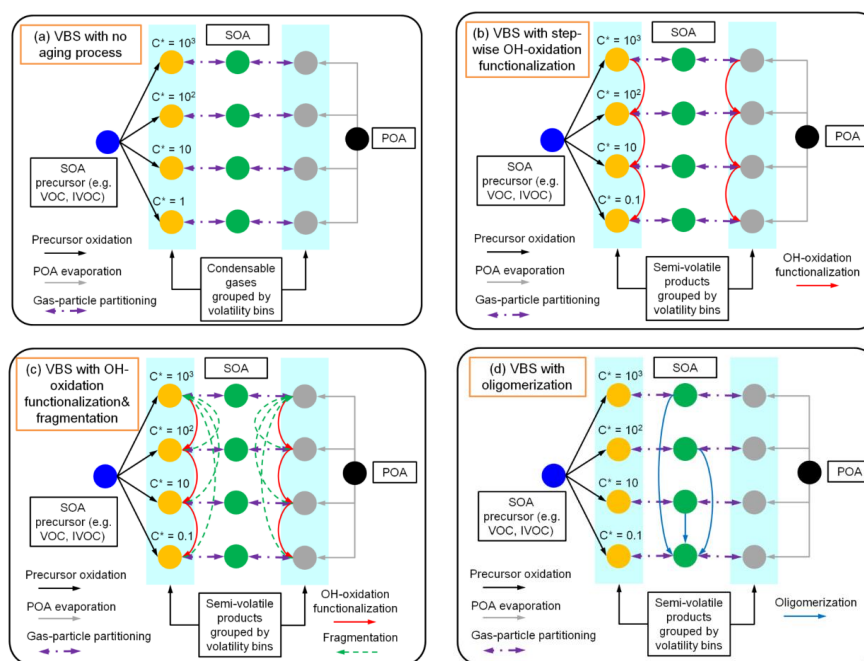
108 differences among schemes/models. Direct comparisons of simulated SOA

109 concentrations across different CTMs can be both time-consuming and resource-

110 intensive. Furthermore, variations in other model configurations, such as physical



111 processes, may obscure the distinctions associated with the SOA schemes themselves.  
112 To address this issue, we performed offline calculations outside the selected CTMs to  
113 focus on SOA formation and aging processes, as described in Section 2. Details of each  
114 SOA model/scheme reviewed are presented in Section 3. Section 4 provides a  
115 comparative analysis of initial (i.e. non-aged) SOA yields from typical precursors as  
116 simulated by each model/scheme. Furthermore, we explore how SOA aging is treated  
117 by different schemes and how NO<sub>x</sub> conditions impact SOA yields. Results from this  
118 study underscore the variability in SOA yields and highlight the need for careful  
119 consideration of model selection and application in the context of air quality studies.  
120



121 **Figure 2** Illustration of VBS schemes with alternative treatments of aging: (a)  
122 no aging; (b) with step-wise OH oxidation causing functionalization only; (c) with  
123 OH-oxidation causing both functionalization and fragmentation; and (d) with  
124 condensed-phase oligomerization.



## 125 **2. Methods**

### 126 **2.1 CTMs and SOA schemes reviewed**

127 To understand the current state of SOA modelling in CTMs, we reviewed schemes  
128 implemented in several regional models that are used in the U.S., Europe, and Asia as well as  
129 one global model. We review eight SOA schemes implemented in five models, namely the  
130 Comprehensive Air Quality with Extensions (CAMx, <https://www.camx.com/>, accessed on Feb  
131 15<sup>th</sup>, 2024), the Community Multiscale Air Quality (CMAQ,  
132 <https://github.com/USEPA/CMAQ/>, accessed on Feb 15<sup>th</sup>, 2024), GEOS-Chem ([https://geos-  
133 chem.readthedocs.io/en/stable/](https://geos-chem.readthedocs.io/en/stable/), accessed on Feb 15<sup>th</sup>, 2024), WRF-Chem  
134 (<https://ruc.noaa.gov/wrf/wrf-chem/>, accessed on Feb 15<sup>th</sup>, 2024), and CHIMERE  
135 (<https://www.lmd.polytechnique.fr/chimere/docs/>, accessed on Feb 15<sup>th</sup>, 2024). For each  
136 model/scheme (hereafter “scheme” for simplicity), we reviewed the official documentation  
137 (e.g., user’s guide), peer-reviewed publications, and, in some cases, the model source code to  
138 understand each SOA parameterization and gather parameter data. Most schemes consider SOA  
139 formation from anthropogenic VOC (AVOC), IVOC, and biogenic VOC (BVOC). Some  
140 schemes also account for the impact of sunlight exposure and/or atmospheric oxidation on SOA  
141 formation/destruction, which is generally referred to as “SOA aging”. Table S1 provides  
142 general information for each SOA model/scheme with more detailed information presented in  
143 Section 3.

### 144 **2.2 Offline calculation of initial SOA yields**

145 The direct comparison of simulated SOA concentrations across different schemes through  
146 conducting full simulations is time-consuming and uncertain because configuring all models  
147 consistently is challenging. Furthermore, differences in the non-SOA physical and chemical  
148 processes between models may obscure the distinctions attributable specifically to the SOA  
149 schemes themselves. To address this issue, an offline calculation (Huang et al., 2023, 2024) is  
150 employed to compare the initial SOA yield (i.e., prior to any aging effects) associated with  
151 different precursors across various schemes. For a two-product scheme, the initial SOA yield  
152 ( $Y$ ) is calculated by combining the gas-particle partitioning theory with the stoichiometric



153 coefficients  $\alpha_i$ :

$$Y = \frac{\alpha_1}{1 + C_1^*/C_{OA}} + \frac{\alpha_2}{1 + C_2^*/C_{OA}} \quad \text{Eq. 1}$$

154 where  $C_{OA}$  is the total ambient concentration of organic compounds (i.e., POA + SOA) and  $\alpha_1$ ,  
155  $\alpha_2$ ,  $C_1^*$ , and  $C_2^*$  represent the stoichiometric coefficients and the effective saturation  
156 concentrations of the above two products, which is obtained by fitting the results of laboratory  
157 studies. Similarly, for a four-bin VBS scheme with no aging effects (e.g. Figure 2a), the SOA  
158 yield is calculated as:

$$Y = \frac{\alpha_1}{1 + 1/C_{OA}} + \frac{\alpha_2}{1 + 10/C_{OA}} + \frac{\alpha_3}{1 + 100/C_{OA}} + \frac{\alpha_4}{1 + 1000/C_{OA}} \quad \text{Eq. 2}$$

159 where  $\alpha_i$  is the initial oxidation yield for each volatility bin  $i$  ( $i=1,2,3,4$ ). Utilizing either Eq. 1  
160 or Eq. 2, the SOA yields under high- and low- $\text{NO}_x$  conditions can be determined at 298 K and  
161 total OA concentrations ranging from 0.1  $\mu\text{g}/\text{m}^3$  to 50  $\mu\text{g}/\text{m}^3$ , using the stoichiometric  
162 coefficients provided by each scheme (listed in Table S2-S9). The initial SOA yield  $Y$  is always  
163 calculated as mass-based in this study while the stoichiometric coefficients  $\alpha_i$  could either be  
164 expressed in mass-base (g/g) or molar-base (ppm/ppm). The initial SOA yields for CMAQ  
165 CRACMM are calculated slightly differently (details presented in Section 3.2.2), given its  
166 special treatment of partially combining gas-phase chemistry and SOA formation. Our analysis  
167 included calculations for anthropogenic precursors (benzene, toluene, and xylene), IVOC and  
168 biogenic precursors (isoprene, monoterpene, and sesquiterpenes).

### 169 **2.3 The effect of SOA aging**

170 Some schemes, such as CAMx two-product and GEOS-Chem Simple, do not account for SOA  
171 aging while others adopt varying approaches to represent the aging process (for a  
172 comprehensive discussion, refer to Section 3). For schemes that include aging effects, we  
173 calculated the aged SOA yields for each precursor at a given time  $t$  by summing over the  
174 particle fraction of all the relevant volatility bins ( $i$ ) using Eq. 3:

$$\text{Aged SOA yields}|_t = \sum_n (f_{particle}^i \cdot \text{SOA mass}|_t^i) \quad \text{Eq. 3}$$

175 where  $f_{particle}^i$  is the particle-phase fraction of each volatility bin (calculated based on Eq. 4)  
176 and  $\text{SOA mass}|_t^i$  is the bin total SOA mass (gas-phase + particle-phase) at time  $t$ ;  $n$  is the total



177 number of bins.

$$f_{particle}^i = \frac{1}{1 + C_i^*/C_{OA}} \quad \text{Eq. 4}$$

178 For gas-phase OH-oxidation style aging (e.g., **Figure 2b** and 2c), the SOA mass is stepped

179 through time ( $\Delta t = t - (t-1)$ ) as follows:

$$\begin{aligned} \text{SOA mass}_t^i &= \text{SOA mass}_{t-1}^i \times (f_{particle}^i + f_{gas}^i \cdot e^{-k_{OH}^*[OH]*\Delta t}) + \\ &\sum_n [\text{SOA mass}_{t-1}^k \times f_{gas}^k \cdot (1 - e^{-k_{OH}^*[OH]*\Delta t}) \times \alpha_k^i] \end{aligned} \quad \text{Eq. 5}$$

180 The first term on the right hand side is the SOA mass in volatility bin ( $i$ ) from the previous time

181 step ( $t-1$ ) multiplied by the fractions that remain after  $\Delta t$  in the particle-phase ( $f_{particle}^i$ ) and

182 gas-phase ( $f_{gas}^i \cdot e^{-k_{OH}^*[OH]*\Delta t}$ ;  $f_{gas}^i = 1 - f_{particle}^i$ ) considering OH-oxidation. The second

183 term is the SOA mass gain from OH-oxidation summed across all  $n$  volatility bins. Here,  $\alpha_k^i$

184 is the mass yield coefficient from bin  $k$  to bin  $i$  and the term  $f_{gas}^k \cdot (1 - e^{-k_{OH}^*[OH]*\Delta t})$  is the gas-

185 phase fraction of SOA in bin  $k$  oxidized by OH during  $\Delta t$ .

186 For particle-phase oligomerization-style aging (e.g. Figure 2d and the CMAQ AERO7 scheme),

187 the aged SOA yield includes the mass of a non-reactive and non-volatile oligomer bin (OLIG)

188 in addition to the semi-volatile bins:

$$\text{Aged SOA yield}_t = \sum_n (f_{particle}^i \cdot \text{SOA mass}_t^i) + \text{SOA mass}_t^{OLIG} \quad \text{Eq. 6}$$

189 The SOA mass (gas-phase + particle-phase) in each volatility bin ( $i$ ) steps through time

190 following Eq. 7 and the mass of the non-volatile oligomer bin ( $\text{SOA mass}_t^{OLIG}$ ) grows with

191 mass-transfer from semi-volatile bins according to Eq. 8:

$$\text{SOA mass}_t^i = \text{SOA mass}_{t-1}^i \times (f_{gas}^i + f_{particle}^i \cdot e^{-k_{OLIG}^*\Delta t}) \quad \text{Eq. 7}$$

$$\begin{aligned} \text{SOA mass}_t^{OLIG} &= \text{SOA mass}_{t-1}^{OLIG} + \\ &\sum_n \{ \text{SOA mass}_{t-1}^i \cdot f_{particle}^i \cdot (1 - e^{-k_{OLIG}^*\Delta t}) \cdot \beta^i \} \end{aligned} \quad \text{Eq. 8}$$

192  $k_{OLIG}$  is the oligomerization rate and  $\beta^i$  is the mass yield coefficient from bin  $i$  to the non-

193 volatile bin OLIG.





194 To compare the aging effects of different schemes, we applied Eq. 3 to Eq. 8 for one day of  
195 aging with an OH concentration of  $3 \times 10^6$  molecules/cm<sup>3</sup> with k<sub>OH</sub> and/or k<sub>OLIG</sub> for each scheme  
196 when applicable. A time step ( $\Delta t$ ) of 0.2 hr was used. Any additional calculations and  
197 assumptions associated with each scheme are further described below.

### 198 **3. Parameterization of SOA scheme in different CTMs**

#### 199 **3.1 CAMx**

200 The Comprehensive Air quality Model with Extensions (CAMx; Emery et al., 2024) is an  
201 Eulerian CTM developed and distributed by Ramboll and version 7.20 was released on May  
202 2<sup>nd</sup>, 2022 (<https://www.camx.com/>, accessed on Feb 15<sup>th</sup>, 2024). CAMx provides two options  
203 to simulate SOA chemistry/partitioning: a “two-product” semi-volatile equilibrium scheme  
204 called SOAP (Strader et al., 1999) and a hybrid 1.5-dimension volatility basis set (1.5-D VBS)  
205 approach (Koo et al., 2014). The former is compatible with advanced probing tools, including  
206 the Particulate Source Apportionment Technology (PSAT) and the decoupled direct method  
207 (DDM), while the latter is not.

##### 208 **3.1.1 CAMx SOAP2**

209 In the CAMx SOAP scheme version 2 (SOAP2), POA is treated as non-volatile and does not  
210 chemically evolve. SOA formation is represented by a modified “two product” model described  
211 above (Figure 1), where gas-phase VOC and IVOC are oxidized to CGs that can condense to  
212 SOA. SOAP2 modifies the two-product scheme by adding a third product, which is considered  
213 non-volatile and always condenses to SOA. The CG products from anthropogenic and biogenic  
214 precursors have different volatilities in SOAP2. Thus, SOAP2 includes 6 product species  
215 overall, as shown in Table S2. The SOA mass yields do not differentiate between different  
216 oxidants (i.e., OH, O<sub>3</sub>, and NO<sub>3</sub>) in SOAP2 and the yield coefficients are fitted to aged SOA  
217 yields (Hodzic et al., 2016). Therefore, no further aging is included in SOAP2. However, SOA  
218 is destroyed in the particle phase by photolysis at a rate of  $0.1\% \times J_{\text{NO}_2}$  (NO<sub>2</sub> photolysis rate).  
219 Aqueous-phase formation of non-volatile SOA from glyoxal and methylglyoxal is also  
220 included with SOAP2.



### 221 3.1.2 CAMx VBS

222 The CAMx hybrid VBS approach, called 1.5-D VBS, combines the simplicity of 1-D VBS  
 223 (Donahue et al. 2006; Robinson et al. 2007) with the ability to describe the evolution of OA in  
 224 both dimensions of oxidation state and volatility (Koo et al. 2014). Unlike SOAP2, CAMx 1.5-  
 225 D VBS treats POA as semi-volatile, and uses two basis sets with five volatility bins ( $C^*$  ranging  
 226 from  $10^{-1}$  to  $10^3 \mu\text{g}/\text{m}^3$  at 298K) to describe SOA formation from anthropogenic and biogenic  
 227 precursors, respectively. Gas-phase oxidation products in different bins are continuously  
 228 oxidized by OH (with a rate constant  $k_{\text{OH}}$  of  $2 \times 10^{-11} \text{ cm}^3 \text{ molecule}^{-1} \text{ s}^{-1}$ ) that move mass from  
 229 higher volatility bins to the next lower volatility bin in a step-wise manner (for example, from  
 230  $C^*=1000 \mu\text{g}/\text{m}^3$  to  $C^*=100 \mu\text{g}/\text{m}^3$  and from  $C^*=100 \mu\text{g}/\text{m}^3$  to  $C^*=10 \mu\text{g}/\text{m}^3$ , as illustrated by  
 231 Figure 2b). For biogenic SOA, this step-wise aging is disabled because over-prediction of OA  
 232 in rural areas was reported (Lane et al., 2008; Murphy and Pandis, 2009). Like SOAP2, SOA  
 233 is destroyed by particle-phase photolysis at a rate of  $0.1\% \times J_{\text{NO}_2}$ . Table S3 shows the parameters  
 234 used for the CAMx 1.5-D VBS scheme. The SOA yields from  $\text{NO}_3$ -initiated monoterpene  
 235 oxidation are different from OH-initiated oxidation and the SOA yields for monoterpenes and  
 236 IVOC are  $\text{NO}_x$ -independent. CAMx 1.5-D VBS differentiates SOA yields from different  
 237 IVOC sources: gasoline engines (IVOG), diesel engines (IVOD), biomass burning (IVOB),  
 238 and other anthropogenic sources (IVOA). SOA yields for IVOD, IVOB and IVOA are the same  
 239 and we only present results for IVOA in this study. Aqueous-phase formation of non-volatile  
 240 SOA from glyoxal and methylglyoxal is also included in the CAMx 1.5D VBS.

### 241 3.2 CMAQ

242 The Community Multiscale Air Quality (CMAQ) model is developed and distributed by the  
 243 US Environmental Protection Agency (EPA). The version CMAQ v5.4 released in October  
 244 2022 offers three SOA options: AERO7 inherited from earlier versions (Appel et al., 2021),  
 245 CRACMM (Pye et al., 2023) introduced in v5.4 for the first time, and a 2D-VBS developed by  
 246 Tsinghua University (<https://github.com/USEPA/CMAQ/tree/2DVBS>, accessed Feb 15<sup>th</sup>,  
 247 2024). We reviewed the first two schemes because both were developed by EPA to support air  
 248 quality planning in the U.S. and elsewhere.



249 3.2.1 CMAQ AERO7

250 The CMAQ AERO7 introduced in version 5.3 (Appel et al. 2021) tracks SOA formation from  
251 anthropogenic VOC (benzene, alkanes, aromatics, polycyclic aromatic hydrocarbons (PAHs)),  
252 biogenic VOC (isoprene,  $\alpha$ -pinene, monoterpenes, and sesquiterpenes), and IVOC.  
253 Additionally, AERO7 accounts for in-cloud SOA formation from glyoxal and methylglyoxal  
254 and aerosol aqueous-phase SOA formation from glyoxal, methylglyoxal and isoprene  
255 epoxydiols (IEPOX). AERO7 scheme employs VBS-based approaches to represent SOA  
256 yields from different precursors, with varying volatility ranges for each precursor. Table S4 to  
257 Table S6 list the AERO7 SOA yields for precursors considered in this study. Specifically,  
258 AERO7 uses a VBS approach with four bins ( $C^*$  ranging from  $0.01 \mu\text{g}/\text{m}^3$  to  $100 \mu\text{g}/\text{m}^3$  at  
259 298K, Table S4) to represent SOA formation from anthropogenic VOC precursors (e.g.,  
260 benzene, long alkanes, PAHs) and seven bins ( $C^*$  ranging from  $0.01$  to  $10^7 \mu\text{g}/\text{m}^3$  at 298K,  
261 Table S5) for  $\alpha$ -pinene and monoterpenes. Isoprene and sesquiterpene oxidation products are  
262 parameterized with two and one semivolatile products (Table S6), respectively. IVOC in  
263 CMAQ is represented by model species pcVOC, which oxidizes with OH to form a low-  
264 volatility condensable vapor (pcSOG,  $C^*=10^{-5} \mu\text{g}/\text{m}^3$ ) with a molar yield of 1 (Murphy et al.  
265 2017, Table S6).

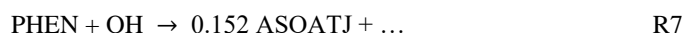
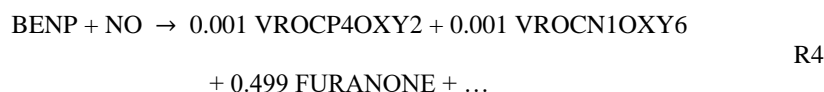
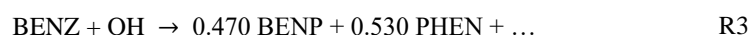
266 AERO7 incorporates aging treatments for SOA that vary by precursor as detailed in Table S10.  
267 SOA formed from AVOC, isoprene, and sesquiterpenes undergo oligomerization in the  
268 particle-phase to form non-volatile SOA (as illustrated by Figure 2d) with a static rate constant  
269  $k_{\text{OLIG}}$  of  $9.49 \times 10^{-6} \text{ s}^{-1}$  (equivalent to a lifetime of  $\sim 30$  hr). In contrast, no oligomerization occurs  
270 for SOA formed from OH-initiated monoterpene oxidation, while SOA formed from  $\text{NO}_3$ -  
271 initiated monoterpene oxidation is subject to particle-phase hydrolysis to non-volatile SOA  
272 with a rate constant of  $9.25 \times 10^{-5} \text{ s}^{-1}$  (equivalent to a lifetime of 3 hr). Unlike CAMx, SOA  
273 photolysis is not considered in AERO7.

274 3.2.2 CMAQ CRACMM

275 The Community Regional Atmospheric Chemistry Multiphase Mechanism (CRACMM) was  
276 introduced in CMAQv5.4 (Pye et al., 2023). Unlike other SOA schemes, CRACMM partially  
277 integrates CG formation and CG aging with oxidant formation in the gas-phase chemical



278 mechanism. Consequently, SOA formation occurs through multiple sequential reactions (as  
279 illustrated below for benzene), meaning that the SOA yield parameters are too complex to be  
280 tabulated for CRACMM in contrast to the other schemes reviewed here. CRACMM SOA  
281 formation considers a comprehensive range of reactive organic carbon (ROC) precursors,  
282 including alkane-like ROC, aromatics, furans, isoprene, monoterpenes, sesquiterpenes, glyoxal  
283 and methylglyoxal. Furthermore, CRACMM categorizes IVOC based on functional groups to  
284 aromatic IVOC, oxygenated IVOC, and alkane IVOC. Aqueous SOA formation from IEPOX,  
285 glyoxal, and methylglyoxal follow CMAQ AERO7.  
286 SOA formation from the OH-initiated oxidation of benzene (BENZ in CRACMM) is shown  
287 here as an example where only the SOA-related products are identified (R3 to R7):



288 Non-volatile products (e.g. ASOATJ in this example) always form 100% SOA. In contrast,  
289 semi-volatile products (e.g. VROCP4OXY2 and VROCN1OXY6) can react further with OH  
290 in the gas-phase and undergo functionalization and/or fragmentation within a simplified 2-D  
291 VBS. By employing a straightforward application of linear algebra, we can multiply the  
292 stoichiometric coefficients of sequential reaction steps (i.e., R3 to R7 for benzene) under both  
293 high and low NO<sub>x</sub> conditions. This approach results in SOA yields that align closely with the  
294 values of Pye et al. (2023) for the average of high and low NO<sub>x</sub> conditions. However, this  
295 algebraic calculation assumes 100% reaction of the precursor and all intermediate products,  
296 such as phenol (PHEN) and furanone. In reality, intermediate products react sequentially with  
297 varying reaction rates (e.g., R3 to R7) that are influenced by the concentrations of OH, HO<sub>2</sub> or  
298 NO. For illustration, we present detailed calculations of aged SOA formation for CRACMM  
299 benzene and  $\alpha$ -pinene in Section S1. As shown by these calculations, the initial SOA yields in



300 CRACMM are zero and thus were excluded from the discussion of initial yields in Section 4.1.

301 As the reactions progress, however, SOA yields begin to rise, demonstrating the importance of  
302 aging to CRACCM. Like CMAQ AERO7, SOA photolysis is not accounted for in CRACMM.

### 303 **3.3 GEOS-Chem**

304 GEOS-Chem is a global chemical transport model driven by meteorological input from the  
305 Goddard Earth Observing System (GEOS) of the NASA Global Modeling and Assimilation  
306 Office (<https://zenodo.org/records/10640536>, accessed on March 1<sup>st</sup>, 2024). GEOS-Chem is  
307 widely used for studying air quality and atmospheric chemistry. Two SOA schemes are  
308 available within GEOS-Chem: a simple scheme and a complex scheme (hereafter GEOS-Chem  
309 Simple and GEOS-Chem Complex) as described by Pai et al. (2020). The former provides  
310 computationally efficient SOA estimates by treating all SOA as non-volatile and using  
311 anthropogenic CO emissions as a surrogate for all anthropogenic SOA precursor emissions.  
312 The latter implements a conventional 1-D VBS framework. The GEOS-Chem Simple scheme  
313 is interesting because it has been shown to replicate atmospheric measurements more  
314 successfully than complex schemes with many more parameters (Nault et al., 2021).

#### 315 **3.3.1 GEOS-Chem Simple scheme**

316 The GEOS-Chem Simple scheme converts a single lumped anthropogenic SOA (ASOA)  
317 precursor to non-volatile SOA with a constant lifetime of 1 day and 100% yield. The  
318 anthropogenic precursor emissions are estimated using CO emissions as a proxy, with scaling  
319 factors of 1.3% and 6.9% for fire/biofuel and fossil fuel sources respectively. This scheme  
320 (Hodzic and Jimenez, 2011; Nault et al., 2021) was developed by comparing ambient  
321 measurements of SOA with CO, which confounds the assumed ASOA yield (100%) with the  
322 derived anthropogenic precursor emission scaling factors (1.3% or 6.9%). Consequently, we  
323 exclude the Simple scheme ASOA yields from some comparisons with other schemes  
324 presented below because the assumption of 100% yield could be considered arbitrary. SOA  
325 formation from IVOC is not explicitly considered in the GEOS-Chem Simple scheme. For  
326 BVOC, the Simple scheme assumes formation of non-volatile biogenic SOA (BSOA) with  
327 constant yields of 3% for isoprene and 10% for monoterpenes and sesquiterpenes. 50% of the



BSOA is formed promptly and the remaining 50% is formed with a constant lifetime of 1.15 days. The Simple scheme has no treatment of SOA aging or SOA photolysis.

### 3.3.2 GEOS-Chem Complex scheme

The GEOS-Chem complex scheme represents SOA formation from anthropogenic and biogenic precursors using a VBS framework. The SOA yields from OH and O<sub>3</sub> initiated oxidation are listed in Table S7 (Pye et al., 2010). This scheme does not include further aging processes (e.g. Figure 2a) and our review of the source code found no treatment of SOA photolysis. SOA formation from IVOC is simulated using naphthalene as a proxy. Additionally, irreversible SOA formation occurs from the aqueous-phase reactive uptake of isoprene (Marais et al., 2016), which is outside the primary focus of the current study.

## 3.4 CHIMERE

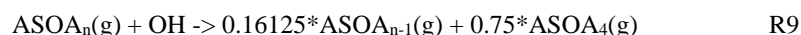
CHIMERE is an Eulerian chemistry-transport model widely used for operational regional air quality forecasts (Honore et al. 2008) and research in Europe (Beekmann and Vautard, 2010; Sciare et al., 2010) as well as other regions of the world (Zhang et al., 2012; Hodzic et al., 2009, 2010; Ma et al., 2019). Version v2023r1 was released in December 2023. Within CHIMERE, three SOA formation schemes are available: single-step oxidation, the Hydrophilic/Hydrophobic Organics (H<sub>2</sub>O) mechanism (Couvidat et al., 2018), and a VBS scheme (Zhang et al., 2013; Cholakian et al., 2018). The VBS scheme includes two subsets: one involving only functionalization and the other involving functionalization, fragmentation, and oligomerization (Zhang et al. 2013; Shrivastava et al. 2015).

We reviewed the CHIMERE VBS scheme with functionalization, fragmentation, and oligomerization processes, referred to as CHIMERE VBS. This scheme models SOA precursors using the SAPRC99 VOC lumping scheme (Luecken et al., 2008) and four VBS bins (C\* ranging 1 to 10<sup>3</sup> µg/m<sup>3</sup> at 298K) with corresponding SOA mass yields listed in Table S8 (Zhang et al. 2013; CHIMERE, 2023). The aging processes for AVOC and BVOC are slightly different in CHIMERE VBS but basically follow Figure 2c. For AVOC, the first two generations of gas-phase products undergo OH-initiated functionalization oxidation with a 7.5% mass gain to account for oxygen addition:

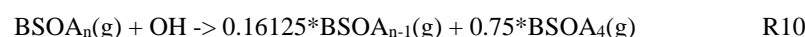




356 Subsequent generations undergo both functionalization (15% yield adjusted for oxygen mass  
357 gain) and fragmentation (75%):



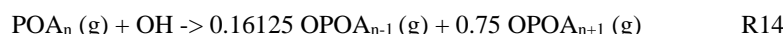
358 Subscript 4 represents the most volatile bin ( $C^* = 10^3 \mu\text{g}/\text{m}^3$  at 298K). Implicitly, R9 assumes a  
359 10% yield of volatile products such as CO or CO<sub>2</sub>. For BVOC, the fragmentation process  
360 occurs from the first generation:



361 In the CHIMERE VBS scheme, both functionalization and fragmentation occur with an OH  
362 rate constant  $k_{\text{OH}}$  of  $1 \times 10^{-11} \text{ cm}^3 \text{ molecule}^{-1} \text{ s}^{-1}$ . Non-volatile SOA (i.e., ANVSOA and  
363 BNVSOA) is formed by oligomerization with a rate constant  $k_{\text{OLIG}}$  of  $3 \times 10^{-4} \text{ s}^{-1}$  corresponding  
364 to a lifetime of 1 hr (R11 and R12).



365 CHIMERE represents IVOC using three high volatility bins of the POA VBS (POA7 to POA9,  
366 corresponding to  $C^* = 10^4$  to  $10^6 \mu\text{g}/\text{m}^3$ ). The IVOC mass fraction assigned to each bin is 24%,  
367 29%, and 47% (Zhang et al. 2013). The gas-phase fraction of each volatility bin undergoes  
368 OH-initiated oxidation to form oxidized POA (OPOA) with lower and/or higher volatility.  
369 Similar to ASOA formation, the first two generations of IV-SOA (SOA formed from IVOC)  
370 undergo only functionalization reactions (with a 7.5% mass gain, R13) while subsequent  
371 generations undergo both functionalization (15% goes to the next lower volatility bin) and  
372 fragmentation (75% goes to the next higher volatility bin, R14):

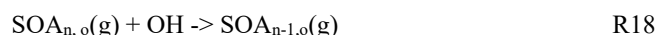
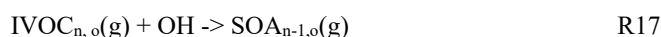
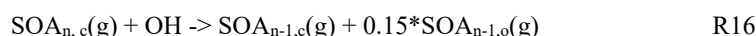
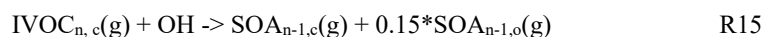


### 373 **3.5 WRF-Chem**

374 WRF-Chem adds atmospheric chemistry to the Weather Research and Forecasting (WRF)  
375 meteorological model to simulate interactions between meteorology and atmospheric  
376 chemistry. Version v4.4 released in April 2022 offers five aerosol schemes (WRF-Chem, 2022):  
377 1) Modal Aerosol Dynamics Model for Europe (MADE/SORGAM, Schell et al. 2001), 2)  
378 Modal Aerosol Dynamics Model for Europe with the VBS (MADE/VBS), 3) Modal Aerosol



379 Module (MAM), 4) Model for Simulating Aerosol Interactions and Chemistry (MOSAIC)  
380 sectional model aerosol parametrization, and 5) bulk aerosol module from GOCART.  
381 We reviewed the MOSAIC scheme as an example of a VBS scheme with functionalization and  
382 fragmentation. In the MOSAIC scheme (Shrivastava et al. 2011), SOA formation from OH-  
383 oxidation is considered but reactions with O<sub>3</sub> and NO<sub>3</sub> radicals are not included. The formation  
384 of SOA from both AVOC and BVOC is modeled using a 4-bin VBS (C\* ranging from 0.1 to  
385 100 µg/m<sup>3</sup> at 298K) with constant yields (Table S9). No additional aging processes are  
386 considered for the condensable gases. SOA photolysis is included in the source code but turned  
387 off by default.  
388 In WRF-Chem, IVOC is represented by three bins, with C\* ranging from 10<sup>4</sup> to 10<sup>6</sup> µg/m<sup>3</sup>. The  
389 formation of SOA from IVOC involves OH-oxidation of both the non-oxygen (with subscript  
390 c) and oxygen parts (with subscript o), with a first-order rate constant k<sub>OH</sub> of 4×10<sup>-11</sup> cm<sup>3</sup>  
391 molecule<sup>-1</sup> s<sup>-1</sup>. For the non-oxygen part, oxidation results in formation of non-oxygen and  
392 oxygen parts (with 15% mass gain) with lower volatility (R15 and R16). At the same time, the  
393 oxygen parts oxidize with OH and move to a lower volatility bin (R17 and R18). Therefore, at  
394 any time both non-oxygen and oxygen parts move to successively lower volatility bins. The  
395 lowest volatility species (C\* = 0.01 µg/m<sup>3</sup>) are assumed to be inert and have no fragmentation  
396 reactions.



## 397 4. Results

### 398 4.1 Comparison of initial SOA yields

399 Initial SOA mass yields (g/g) for all schemes (except CMAQ CRACMM) are summarized in  
400 Table 1. Initial refers to the yields immediately following precursor oxidation and before any  
401 subsequent SOA aging process. Since mass yields can vary with C<sub>OA</sub>, we assume C<sub>OA</sub> of 10  
402 µg/m<sup>3</sup> in Table 1, which is relevant to ambient air quality and often used as a reference C<sub>OA</sub> for  
403 SOA yield comparisons. The ratio of maximum to minimum initial SOA yields for a same





precursor shows wide variations across different schemes, with the least variation (factor of 1.8) observed for monoterpene at low NO<sub>x</sub> conditions and over three orders of magnitude for IVOC (factor of 3715). These variations can become greater when C<sub>OA</sub> is either increased or decreased from 10 µg/m<sup>3</sup> (as assumed for Table 1) and when effects of aging processes on initial yields are included (as shown in Section 4.2).

#### 4.1.1 Initial SOA yields from anthropogenic VOC

Figure 3 shows how the initial SOA mass yields depend on C<sub>OA</sub> for three anthropogenic VOC (AVOC), namely benzene (BENZ), toluene (TOL), and xylene (XYL). For WRF-Chem and CHIMERE, the SOA yields for model species ARO1 are used to represent BENZ and TOL whereas those of ARO2 are used for XYL. As illustrated by Figure 3, the SOA yields from aromatics generally increase with C<sub>OA</sub>, except for GEOS-Chem Simple. The SOA yields become independent of C<sub>OA</sub> when the product is treated as non-volatile as exemplified by the GEOS-Chem Simple scheme, which assumes constant SOA yields of 100% for all three precursors. Conversely, the SOA yields increase strongly with C<sub>OA</sub> when the SOA is treated as semi-volatile. The CAMx SOAP2 scheme is an intermediate case with SOA yields increasing more gradually with C<sub>OA</sub> than the CHIMERE scheme. CMAQ AERO7 and GEOS-Chem Complex predict almost identical SOA yields (due to close stoichiometric coefficients) and exhibit no dependence on C<sub>OA</sub> under low NO<sub>x</sub> conditions. Overall, schemes consistently show higher ASOA yields from aromatics under low NO<sub>x</sub> than high NO<sub>x</sub> conditions but diverge in the magnitude of these yields (max./min. yields at 10 µg/m<sup>3</sup> ranging from 2.0 to 5.8) and diverge in how yields depend on C<sub>OA</sub> (ranging from independent to strongly increasing).

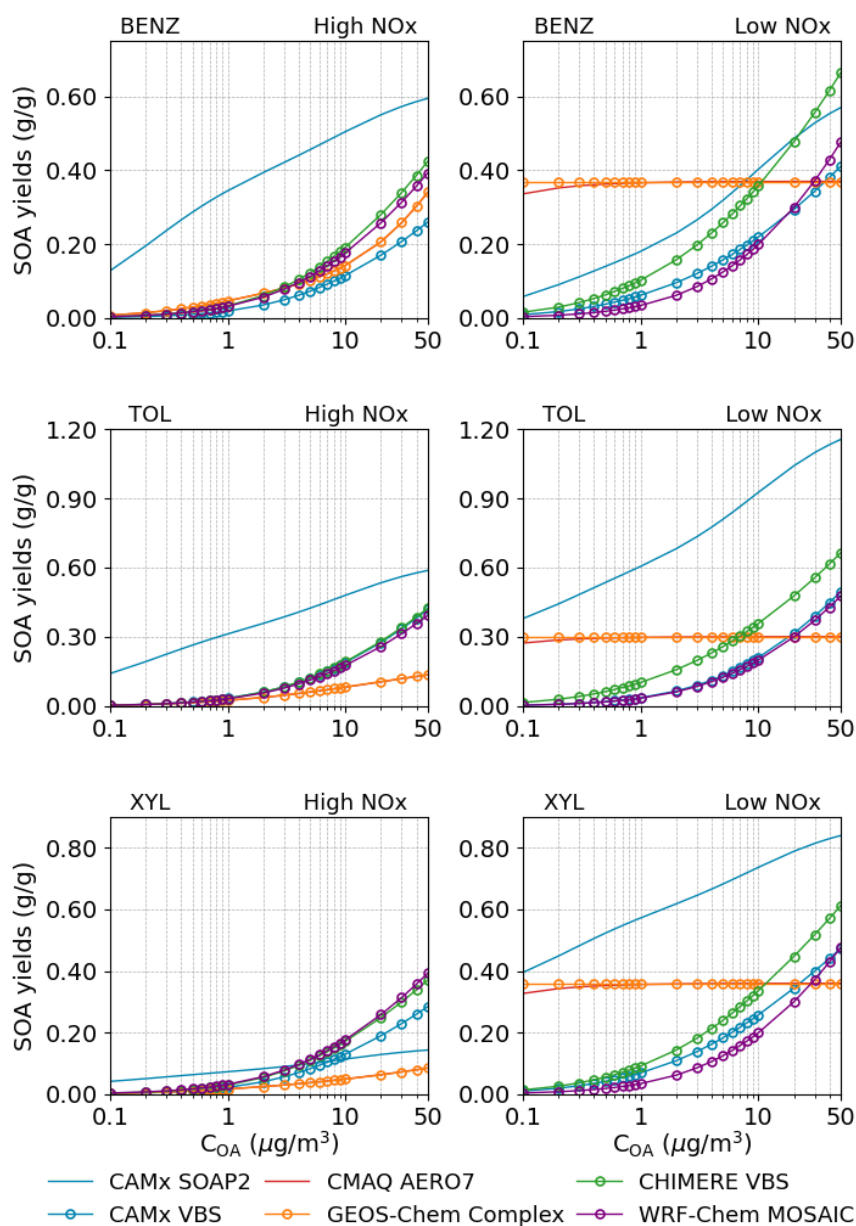


**Figure 3** Comparison of the initial SOA yields (g/g) as functions of  $C_{OA}$  for three anthropogenic VOC among different schemes (CMAQ CRACMM not included). SOA yields are calculated at 298 K.



**Table 1** Initial SOA yields (g/g) for different precursors across schemes at 298 K and  $C_{OA}$  of  $10 \mu\text{g}/\text{m}^3$ .

| Precursor-<br>NOx case  | CMx <sup>1</sup><br>SP2 | CMx<br>VBS | CMQ<br>AE7 | CMQ<br>CRM | G-C<br>Spl | G-C<br>Cpx | CMR<br>VBS               | W-C<br>MOS               | Avg <sup>7</sup> | Max/<br>Min <sup>8</sup> |
|-------------------------|-------------------------|------------|------------|------------|------------|------------|--------------------------|--------------------------|------------------|--------------------------|
| BENZ <sup>2</sup> -high | 0.51                    | 0.12       | 0.14       | 0          | /          | 0.14       | 0.19                     | 0.18                     | 0.21             | 4.4                      |
| BENZ-low                | 0.40                    | 0.22       | 0.37       | 0          | /          | 0.37       | 0.36                     | 0.20                     | 0.32             | 2.0                      |
| TOL <sup>3</sup> -high  | 0.48                    | 0.19       | 0.08       | 0          | /          | 0.08       | 0.19                     | 0.18                     | 0.20             | 5.8                      |
| TOL-low                 | 0.93                    | 0.21       | 0.30       | 0          | /          | 0.30       | 0.36                     | 0.20                     | 0.38             | 4.6                      |
| XYL <sup>4</sup> -high  | 0.11                    | 0.13       | 0.05       | 0          | /          | 0.05       | 0.17                     | 0.18                     | 0.12             | 3.6                      |
| XYL-low                 | 0.74                    | 0.26       | 0.36       | 0          | /          | 0.36       | 0.34                     | 0.20                     | 0.38             | 3.7                      |
| IVOC <sup>5</sup> high  | 0.36                    | 0.51       | 1.00       | 0          | /          | 0.20       | 2.7x<br>10 <sup>-4</sup> | 2.7x<br>10 <sup>-4</sup> | 0.35             | 3715                     |
| IVOC-low                | 0.55                    | 0.51       | 1.00       | 0          | /          | 0.73       | 2.7x<br>10 <sup>-4</sup> | 2.7x<br>10 <sup>-4</sup> | 0.46             | 3715                     |
| ISOP-high               | 0.05                    | 0.01       | 0.05       | 0          | 0.03       | 0.04       | 0.04                     | 0.01                     | 0.03             | 4.0                      |
| ISOP-low                | 0.09                    | 0.03       | 0.05       | 0          | 0.03       | 0.04       | 0.07                     | 0.02                     | 0.05             | 3.8                      |
| TERP-high               | 0.14                    | 0.09       | 0.17       | 0          | 0.10       | 0.09       | 0.13                     | 0.10                     | 0.12             | 1.8                      |
| TERP-low                | 0.21                    | 0.18       | 0.17       | 0          | 0.10       | 0.19       | 0.25                     | 0.18                     | 0.18             | 2.5                      |
| SESQ <sup>6</sup> -high | 0.52                    | 0.22       | 0.44       | 0          | 0.10       | 0.84       | 0.20                     | 0.22                     | 0.36             | 8.4                      |
| SESQ-low                | 0.70                    | 0.22       | 0.44       | 0          | 0.10       | 0.42       | 0.20                     | 0.22                     | 0.33             | 7.0                      |

<sup>1</sup> Model name abbreviations are CMx for CAMx, CMQ for CMAQ, G-C for GEOS-Chem, CMR for CHIMERE, and W-C for WRF-Chem. Scheme name abbreviations are SP2 for SOAP2, AE7 for AERO7, Spl for Simple, Cpx for Complex, and MOS for MOSAIC.

<sup>2</sup> For WRF-Chem and CHIMERE, results for BENZ are based on ARO1.

<sup>3</sup> For WRF-Chem and CHIMERE, results for TOL are based on ARO1.

<sup>4</sup> For WRF-Chem and CHIMERE, results for XYL are based on ARO2. For CMAQ CRACMM, results for XYL are averages of XYE and XYM.

<sup>5</sup> For CMAQ CRACMM, IVOC yields are average of alkane and oxygenated IVOCs (see details in Table S11). For WRF-Chem MOSAIC, IVOC is assumed to have 50% oxygen.

<sup>6</sup> For CHIMERE, results for SESQ are based on humulene.

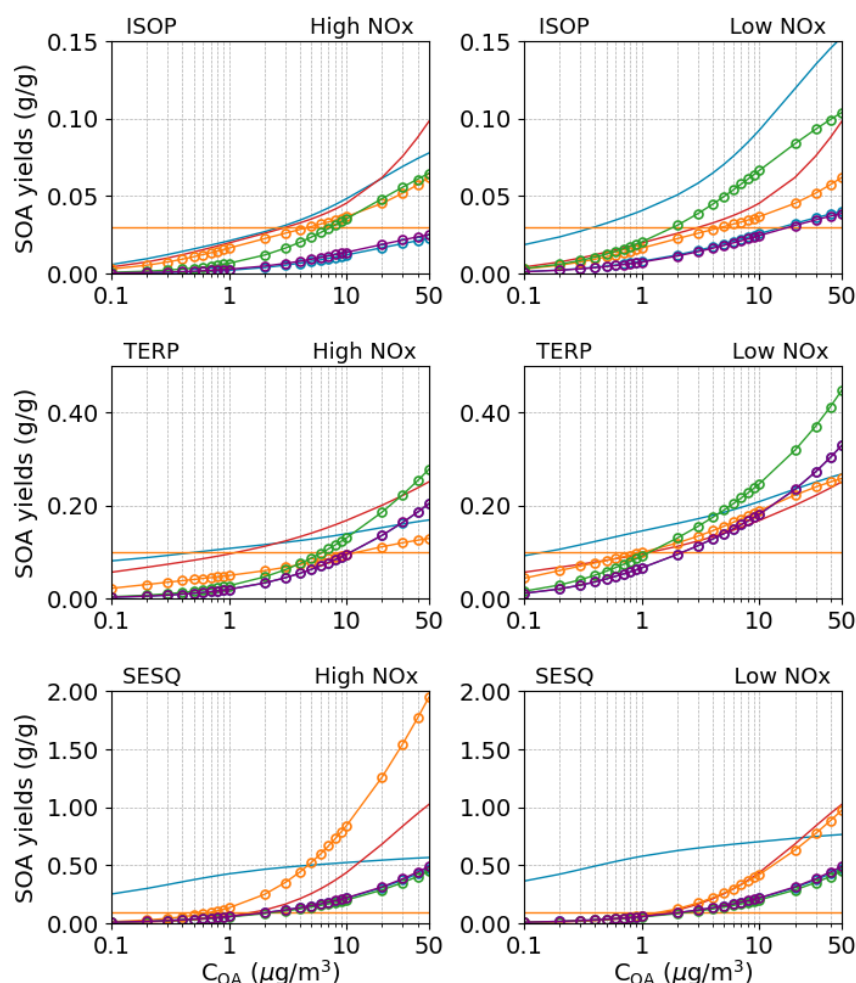
<sup>7</sup> Multi-model average yield excluding GEOS-Chem Simple for aromatics and IVOC, and excluding CRACMM for ISOP.

<sup>8</sup> Ratio of maximum to minimum yield.



446 4.1.2 Initial SOA yields from biogenic VOC

447 Figure 4 shows how the initial SOA mass yields depend on  $C_{OA}$  for three biogenic VOC  
448 (BVOC), namely isoprene (ISOP), monoterpenes (TERP), and sesquiterpenes (SESQ). For  
449 isoprene, CMAQ includes heterogeneous SOA formation from IEPOX (Pye et al., 2013),  
450 which is outside the scope of this evaluation and thus is not discussed in this study.  
451 Overall, the BSOA yield patterns closely resemble those of ASOA. All schemes, except for  
452 GEOS-Chem Simple, predict an increase in yields associated with  $C_{OA}$ . However, the  
453 magnitude of SOA yields varies significantly across schemes, ranging from 1.8 to 8.4 under  
454 high  $NO_x$  conditions and 2.5 to 7.0 under low  $NO_x$  conditions. Additionally, model predictions  
455 regarding the influence of  $NO_x$  on BSOA yields are inconsistent, with some indicating an  
456 increase, others a decrease, and some showing no effect. For instance, SOA yields from ISOP  
457 under high  $NO_x$  conditions, as simulated by two CAMx schemes, WRF-Chem MOSAIC, and  
458 CHIMERE VBS, are approximately half of those under low  $NO_x$  conditions. In contrast,  
459 CMAQ AERO7 and GEOS-Chem schemes suggest that SOA yields are independent of  $NO_x$   
460 levels. Regarding TERP-derived SOA, all schemes, except for CMAQ AERO7 and GEOS-  
461 Chem Simple, predict more than 50% higher yields under low  $NO_x$  conditions compared to  
462 high  $NO_x$  conditions. The latter two schemes show no difference between  $NO_x$  regimes. For  
463 SESQ, four models (CAMx VBS, CMAQ AERO7, CHIMERE VBS, and WRF-Chem  
464 MOSAIC) predict no distinction in SOA yields between high and low  $NO_x$  conditions.  
465 Conversely, CAMx SOAP2 suggests higher yields under low  $NO_x$  conditions, whereas the  
466 GEOS-Chem Complex scheme predicts the opposite.



— CAMx SOAP2 — CMAQ AERO7 — GEOS-Chem Simple — CHIMERE VBS  
— CAMx VBS — GEOS-Chem Complex — WRF-Chem MOSAIC

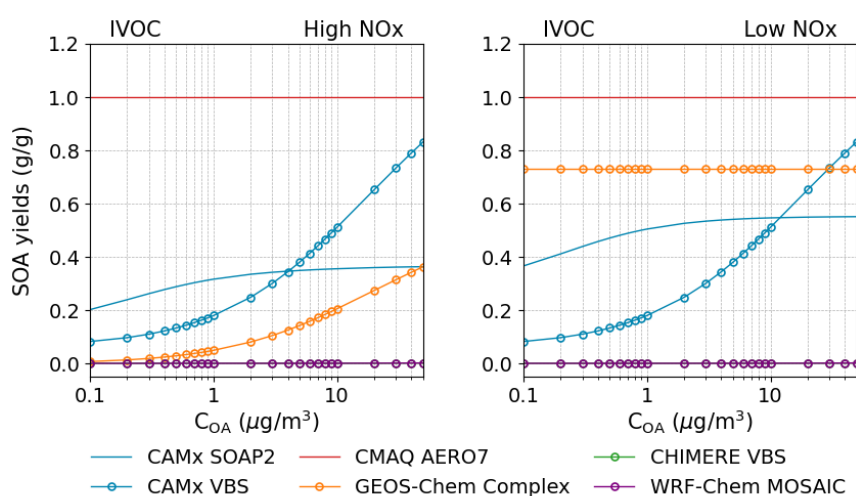
**Figure 4** Comparison of the initial SOA yields (g/g) as functions of  $C_{OA}$  for three biogenic VOC among different schemes (CMAQ CRACMM not included). SOA yields are calculated at 298 K.

#### 4.1.3 Initial SOA yields from intermediate volatility organic compounds (IVOC)

IVOC emissions make important contributions to ASOA formation (Robinson et al., 2016; Ma et al., 2016; Zhao et al., 2014). The SOA yields from IVOC, referred to as IV-SOA, predicted by each scheme are shown in Figure 5. The GEOS-Chem Simple scheme is omitted since it does not explicitly account for IVOC. Additionally, the results for CMAQ CRACMM are discussed separately in Section 4.2.3, due to its distinct treatment of several IVOC types.



477 SOA yields from IVOC in the CAMx VBS scheme shows a strong positive dependence on  $C_{OA}$   
 478 whereas CAMx SOAP2 and GEOS-Chem Complex exhibit much weaker responses. Constant  
 479 SOA yields of 1.0 g/g are set in CMAQ AERO7, regardless of  $NO_x$  levels, surpassing the  
 480 values predicted by other schemes. SOA formation from IVOC in CHIMERE VBS and WRF-  
 481 Chem MOSAIC is treated as multi-generational oxidations (R13-R18), resulting in extremely  
 482 low initial SOA yields (<0.001 g/g).



483

484 **Figure 5** Comparison of the initial SOA yields (g/g) as functions of  $C_{OA}$  for IVOC among  
 485 different schemes (CMAQ CRACMM and GEOS-Chem Simple not included). SOA yields  
 486 are calculated at 298 K.

## 487 4.2 Comparison of SOA aging

488 Among the eight schemes we evaluated, the CAMx SOAP2, GEOS-Chem Simple, and GEOS-  
 489 Chem Complex schemes do not incorporate explicit SOA aging processes. However, the  
 490 SOAP2 yields are derived from a VBS parameterization that includes aging (Hodzic et al.,  
 491 2016) and may therefore be considered pre-aged (Emery et al., 2024). The remaining schemes  
 492 account for SOA aging using one or more of three mechanisms: gas-phase OH-oxidation,  
 493 condensed-phase oligomerization, and condensed-phase hydrolysis. Gas-phase OH-oxidation  
 494 aging is typically parameterized as functionalization reactions that generate less volatile  
 495 products (e.g. **Figure 2b**) and/or fragmentation reactions that produce more volatile products  
 496 (e.g. **Figure 2c**). This mechanism is adopted in CAMx VBS (for AVOC and IVOCs only),



497 CMAQ CRACMM, WRF-Chem MOSAIC and CHIMERE VBS, with implementation being  
498 specific to each scheme. Condensed-phase oligomerization aging (e.g. **Figure 2d**) is  
499 characterized as a first-order particle-phase reaction, usually assuming a lifetime of 30 hr,  
500 leading to non-volatile product formation independent of oxidant concentrations. CMAQ  
501 AERO7 applies this process for SOA formed from all precursors except monoterpenes. For  
502 SOA derived from NO<sub>3</sub> oxidation of monoterpenes, AERO7 instead applies condensed-phase  
503 hydrolysis, yielding non-volatile products with a lifetime of ~3 hr.

504 To compare the aging effects on SOA yields across different schemes, we assumed a 24-hour  
505 exposure to an OH concentration of  $3 \times 10^6$  molecules/cm<sup>3</sup> (equivalent to  $2.6 \times 10^{11}$   
506 molecules·s·cm<sup>-3</sup>) for the OH-oxidation aging process or a 24-hour of condensed-phase  
507 oligomerization/hydrolysis when calculating the aged SOA yields (details presented below).  
508 Table 2 summarizes the aged SOA yields (when applicable) at 298 K with a C<sub>OA</sub> of 10 µg/m<sup>3</sup>  
509 as simulated by each scheme. Figure 6 and Figure 7 further compare the initial and aged SOA  
510 yields for each scheme and SOA precursor, while Figure 8 separately illustrates the aging  
511 effects on IVOC-derived SOA across different schemes.

#### 512 4.2.1 Aging in CAMx VBS

513 The CAMx VBS scheme incorporates step-wise gas-phase OH-oxidation aging for AVOC and  
514 IVOC without accounting for fragmentation processes (**Figure 2b**). The calculation of aged  
515 SOA yields follows Eq. 3 to Eq. 5, using a k<sub>OH</sub> value of  $2 \times 10^{-11}$  cm<sup>3</sup> molecule<sup>-1</sup> s<sup>-1</sup> and an OH  
516 concentration of  $3 \times 10^6$  molecules cm<sup>-3</sup>. Figure 7a-b illustrates how SOA yields change as a  
517 function of accumulated OH exposure under high and low NO<sub>x</sub> conditions for different  
518 precursors. In the CAMx VBS scheme, SOA yields increase with OH exposure though the rate  
519 of aging slows as the OH exposure increases. With a 24-hour period (corresponding to an OH  
520 exposure of  $2.6 \times 10^{11}$  molecules·s·cm<sup>-3</sup>), SOA yields from aromatics increase by a factor of 5-  
521 6 under high NO<sub>x</sub> conditions and 3-5 under low NO<sub>x</sub> conditions compared to their initial yields.  
522 For IVOC, aged SOA yields increase by 125% relative to the initial yields (Figure 8b). These  
523 findings highlight the significant influence of aging processes implemented in the CAMx VBS  
524 scheme.



**Table 2** Aged SOA yields (g/g) for different precursors across schemes at 298 K and  $C_{OA}$  of  $10 \mu\text{g}/\text{m}^3$ . Shaded values indicate no aging effect (i.e. identical to values in Table 1).

| Precursor-<br>NOx case  | CMx <sup>1</sup><br>SP2 | CMx<br>VBS | CMQ<br>AE7 | CMQ<br>CRM | G-C<br>Spl | G-C<br>Cpx | CMR<br>VBS | W-C<br>MOS | Avg <sup>7</sup> | Max/<br>Min <sup>8</sup> |
|-------------------------|-------------------------|------------|------------|------------|------------|------------|------------|------------|------------------|--------------------------|
| BENZ <sup>2</sup> -high | 0.51                    | 0.80       | 0.22       | 0.23       | /          | 0.14       | 0.79       | 0.18       | 0.41             | 5.6                      |
| BENZ-low                | 0.40                    | 1.07       | 0.37       | 0.67       | /          | 0.37       | 1.11       | 0.20       | 0.60             | 5.6                      |
| TOL <sup>3</sup> -high  | 0.48                    | 1.30       | 0.12       | 0.11       | /          | 0.08       | 0.79       | 0.18       | 0.44             | 15.7                     |
| TOL-low                 | 0.93                    | 1.33       | 0.30       | 0.50       | /          | 0.30       | 1.11       | 0.20       | 0.67             | 6.7                      |
| XYL <sup>4</sup> -high  | 0.11                    | 0.83       | 0.07       | 0.09       | /          | 0.05       | 0.66       | 0.18       | 0.29             | 16.9                     |
| XYL-low                 | 0.74                    | 1.14       | 0.36       | 0.51       | /          | 0.36       | 0.98       | 0.20       | 0.61             | 5.7                      |
| IVOC <sup>5</sup> high  | 0.36                    | 1.15       | 1.00       | 0.31       | /          | 0.20       | 0.02       | 1.20       | 0.60             | 73.7                     |
| IVOC-low                | 0.55                    | 1.15       | 1.00       | 0.53       | /          | 0.73       | 0.02       | 1.20       | 0.74             | 73.7                     |
| ISOP-high               | 0.05                    | 0.01       | 0.06       | /          | 0.03       | 0.04       | 0.08       | 0.01       | 0.04             | 6.8                      |
| ISOP-low                | 0.09                    | 0.03       | 0.06       | /          | 0.03       | 0.04       | 0.12       | 0.02       | 0.06             | 5.0                      |
| TERP-high               | 0.14                    | 0.09       | 0.17       | 0.84       | 0.10       | 0.09       | 0.54       | 0.10       | 0.26             | 5.7                      |
| TERP-low                | 0.21                    | 0.18       | 0.17       | 0.20       | 0.10       | 0.19       | 0.80       | 0.18       | 0.25             | 17.5                     |
| SESQ <sup>6</sup> -high | 0.52                    | 0.22       | 0.78       | 0.54       | 0.10       | 0.84       | 0.86       | 0.22       | 0.51             | 8.6                      |
| SESQ-low                | 0.70                    | 0.22       | 0.78       | 1.04       | 0.10       | 0.42       | 0.86       | 0.22       | 0.54             | 10.4                     |

<sup>1</sup> Model name abbreviations are CMx for CAMx, CMQ for CMAQ, G-C for GEOS-Chem, CMR for CHIMERE, and W-C for WRF-Chem. Scheme name abbreviations are SP2 for SOAP2, AE7 for AERO7, Spl for Simple, Cpx for Complex, and MOS for MOSAIC.

<sup>2</sup> For WRF-Chem and CHIMERE, results for BENZ are based on ARO1.

<sup>3</sup> For WRF-Chem and CHIMERE, results for TOL are based on ARO1.

<sup>4</sup> For WRF-Chem and CHIMERE, results for XYL are based on ARO2. For CMAQ CRACMM, results for XYL are averages of XYE and XYM.

<sup>5</sup> For CMAQ CRACMM, IVOC yields are average of alkane and oxygenated IVOCs (see details in Table S11). For WRF-Chem MOSAIC, IVOC is assumed to have 50% oxygen.

<sup>6</sup> For CHIMERE, results for SESQ are based on humulene.

<sup>7</sup> Multi-model average yield excluding GEOS-Chem Simple for aromatics and IVOC, and excluding CRACMM for ISOP.

<sup>8</sup> Ratio of maximum to minimum yield.



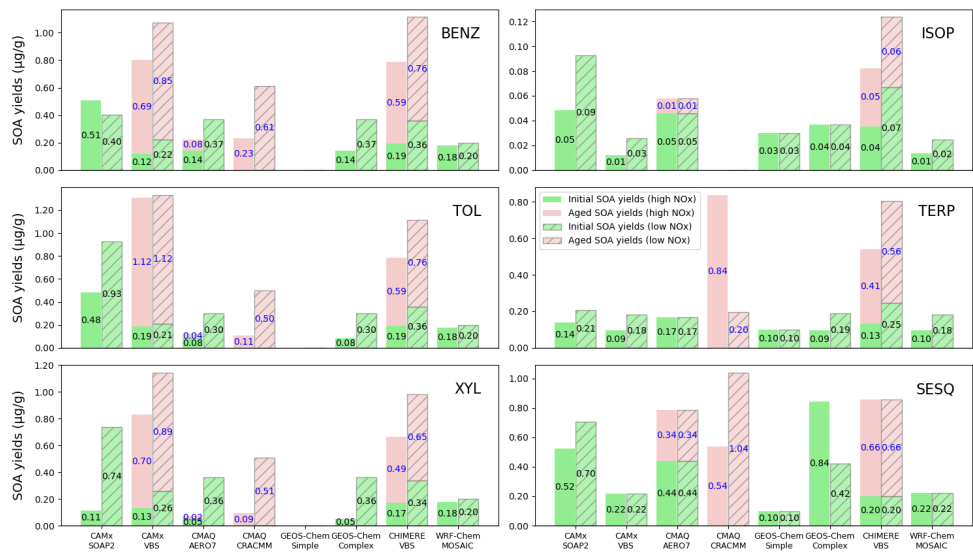


**Figure 6** Effect of aging on SOA yields (g/g) for different precursors under high and low NOx conditions.



545 4.2.2 Aging in CMAQ AERO7

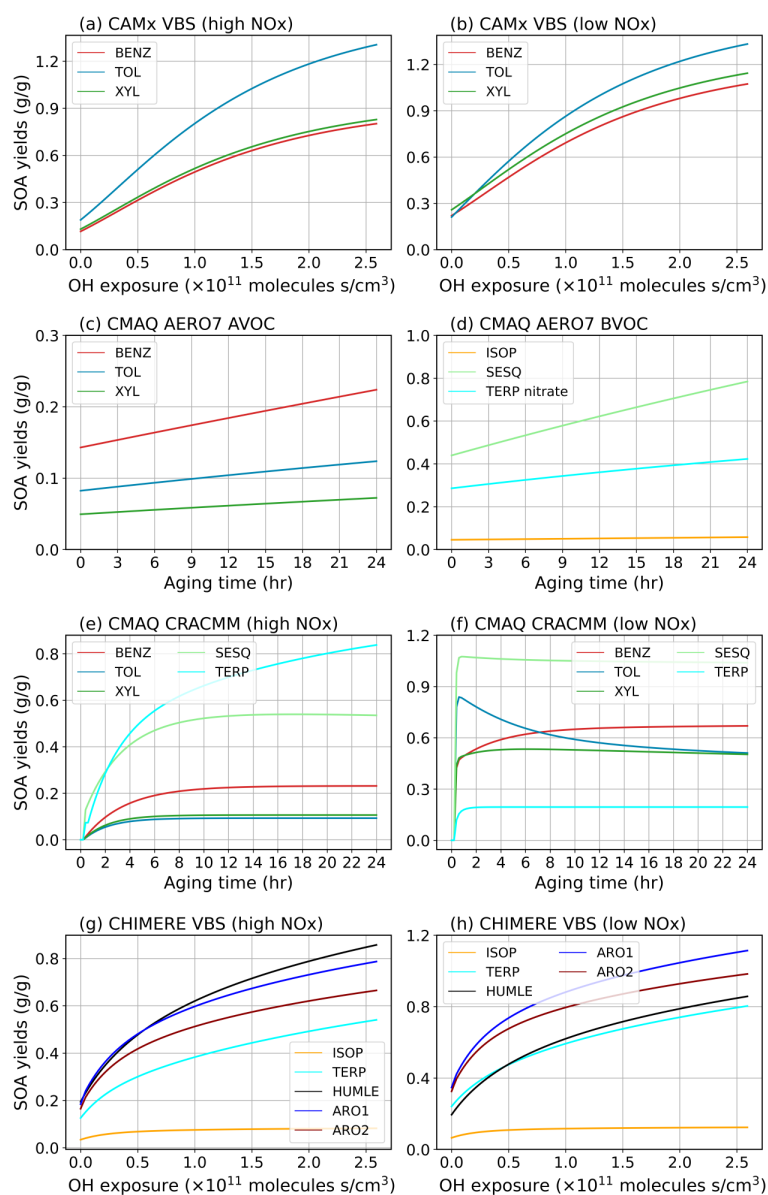
546 The SOA aging process in the CMAQ AERO7 scheme involves particle-phase  
547 oligomerization (**Figure 2d**) and hydrolysis. Oligomerization applies to SOA formed  
548 from ISOP, SESQ, and aromatics (only under high-NO<sub>x</sub> conditions) while hydrolysis  
549 affects SOA formed from monoterpenes oxidation by NO<sub>3</sub> radical. The aged SOA  
550 yields resulting from oligomerization and hydrolysis follows Eq. 6 to Eq. 8, with rate  
551 constants  $k_{\text{OLIG}} = 9.49 \times 10^{-6} \text{ s}^{-1}$  and  $k_{\text{hydro}} = 9.26 \times 10^{-5} \text{ s}^{-1}$ . Figure 7b illustrates the  
552 evolution of SOA yields over 24 hours of oligomerization, showing increases of 27%,  
553 79%, and 46%-57% for ISOP, SESQ, and aromatics, respectively. This increase results  
554 from the reduced volatility of SOA due to oligomerization. The hydrolysis reaction,  
555 assuming a shorter lifetime of approximately 3 hr, leads to a 48% increase in SOA yield  
556 from monoterpene-derived organic nitrates over 1 day. Although the hydrolysis rate is  
557 nearly ten times faster than that of oligomerization, the overall yield increase is  
558 moderated because the hydrolysis products have lower molecular weights than their  
559 parent compounds.

560 4.2.3 Aging in CMAQ CRACMM

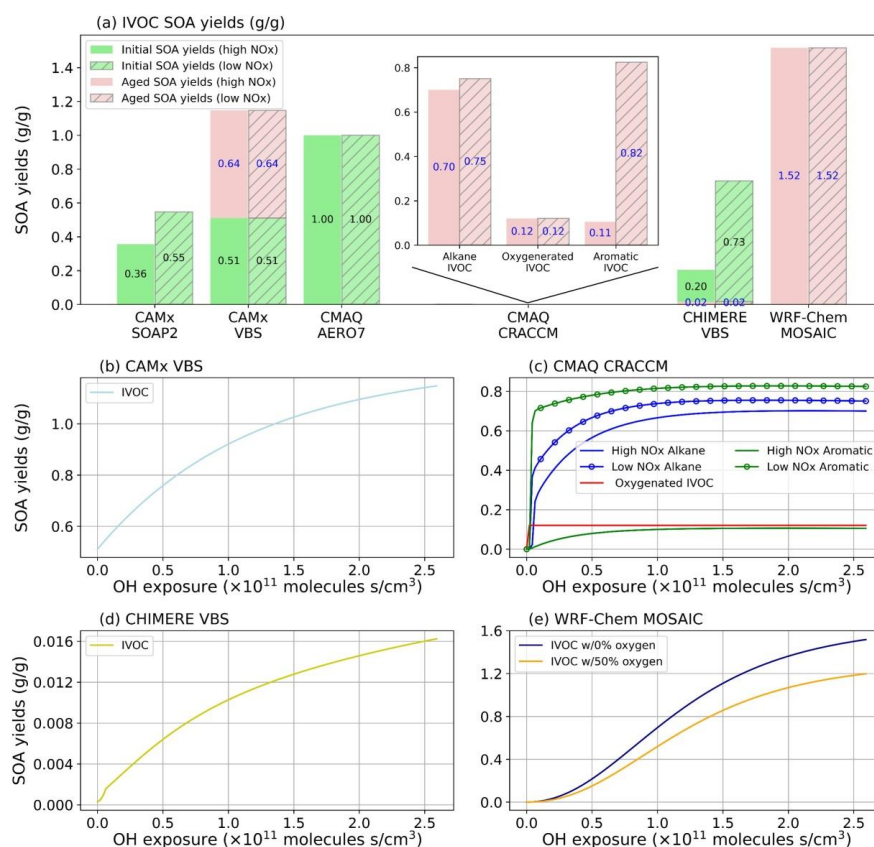
561 The aging processes in CMAQ CRACMM involve the gas-phase OH-oxidation  
562 reactions of secondary oxygenated L/S/IVOCs, leading to both fragmentation and  
563 functionalization, and resulting in products with varying volatilities. As illustrated in  
564 Figure 7e-f, the impact of aging on SOA yields depends on the precursor and varies  
565 between high NO<sub>x</sub> and low NO<sub>x</sub> conditions. Under high NO<sub>x</sub> conditions, SOA yields  
566 from all precursors increase substantially during the first 6-8 hours, after which the  
567 growth rate becomes negligible (except for TERP, which continues to increase). After  
568 24 hours of aging, SOA yields under high NO<sub>x</sub> conditions range from 0.093 g/g for  
569 XYL to 0.838 g/g for TERP (Table 2). In contrast, under low NO<sub>x</sub> conditions, all  
570 precursors show a sharp increase in SOA yields within the first 30 mins. Subsequently,  
571 SOA yields from XYL begin to decline, gradually reaching a minimum value of  
572 approximately 0.511 g/g after 16 hours. On the contrary, BENZ yields continue to  
573 increase slightly, peaking around 0.670 g/g. TERP, TOL, and SESQ yields exhibit



574 minimal change after their initial increase. After 24 hours, SOA yields under low NO<sub>x</sub>  
575 conditions range from 0.195 g/g for TERP to 1.039 g/g for SESQ.



576  
577 **Figure 7** Effect of aging on SOA yields (g/g) from different precursors as a function  
578 of OH exposure or aging time in different schemes. (a-b) CAMx VBS; (c-d) CMAQ  
579 AERO7; (e-f) CMAQ CRACMM; and (g-h) CHIMERE VBS. The numbers in the  
580 brackets indicate the relative change of SOA yields at hour 24 to hour 0.



581

582 **Figure 8** Effect of aging on SOA yields (g/g) for IVOC precursors under high and  
583 low NO<sub>x</sub> conditions for different schemes.

584 Unlike other schemes, the CMAQ CRACMM scheme classifies IVOC into alkanes,  
585 aromatics, and oxygenated IVOC based on their functional groups. Emitted oxygenated  
586 IVOC do not exhibit aging effects, as their oxidation products are assumed to be non-  
587 volatile (Figure 8c). In contrast, SOA yields from alkane and aromatic IVOC increase  
588 with the aging time, with the growth rate becoming negligible after approximately 10  
589 hours. SOA yields from oxygenated IVOC (0.121 g/g) are independent of NO<sub>x</sub>  
590 conditions. The other two IVOC types show higher SOA yields under low NO<sub>x</sub>  
591 conditions, particularly for aromatic IVOC, where the SOA yields under low NO<sub>x</sub>  
592 conditions (0.825 g/g) are nearly 8 times that under high NO<sub>x</sub> conditions (0.105 g/g).



#### 593 4.2.4 Aging in CHIMERE VBS

594 The CHIMERE VBS scheme accounts for aging through gas-phase functionalization  
595 and fragmentation, as well as condensed-phase oligomerization, as shown in R9 to R12.  
596 Figure 7d presents the combined aging effects on SOA over a 24-hour period under this  
597 scheme. Among BVOC, the aging effect is more pronounced for TERP and humulenes  
598 (HUMULE) than for ISOP. Under high NO<sub>x</sub> conditions, the SOA yields from ISOP,  
599 TERP, and HUMULE increase by 141%, 331%, and 341%, respectively, over one day.  
600 In contrast, under low NO<sub>x</sub> conditions, the aging effect is generally less significant,  
601 except for HUMULE, which exhibits a similar level of aging under both NO<sub>x</sub> regimes.  
602 Aromatics show substantial increase in SOA yields—over 300% under high NO<sub>x</sub> and  
603 200% under low NO<sub>x</sub> conditions.

604 Aging of SOA from IVOC results in a dramatic increase in yields—by nearly a factor  
605 of 60 within one day, as shown by Figure 8d. However, the absolute SOA yields from  
606 IVOC remain low (approximately 0.01 g/g), which is attributed to the initial low SOA  
607 formation ( $\sim 10^{-4}$  g/g) and the dominance of fragmentation at higher oxidation  
608 generations. From the third oxidation generation onward, 75% of the condensable gases  
609 undergo fragmentation into more volatile products, while only 15% undergo  
610 functionalization, as described in R14.

#### 611 4.2.5 Aging in WRF-Chem MOSAIC

612 The WRF-Chem MOSAIC scheme does not include SOA aging processes for AVOC  
613 and BVOC. SOA formation from IVOC is parameterized as a stepwise gas-phase OH-  
614 oxidation process. For the non-oxygen component of condensable gases, a 15% mass  
615 gain is assumed for each generation (as per R15 and R16). Meanwhile, the oxygenated  
616 component shifts to lower volatility bins without mass gain (as per R17 and R18). The  
617 scheme does not consider fragmentation or condensed-phase oligomerization. Figure  
618 8e illustrates aging effects under two scenarios: IVOC with hydrocarbon-like  
619 characteristics (0% oxygen by mass at  $t=0$ , representing of diesel emissions) and IVOC  
620 with 50% oxygen by mass (representing of biomass burning emissions). In both cases,  
621 the non-fragmenting stepwise aging process in WRF-Chem results in substantial



622 increases in SOA yields. At an OH exposure of  $2.6 \times 10^{11}$  molecule·s·cm<sup>-3</sup> (i.e. a 24-hour  
623 period), SOA formed from hydrocarbon-like IVOC exceeds 1 g/g, despite an initially  
624 negligible yield.

### 625 **4.3 NO<sub>x</sub> effects on SOA yields**

626 Evaluating SOA yields for seven precursor types across eight modeling schemes results  
627 in 56 potential characterizations of how NO<sub>x</sub> levels influence SOA formation. Table  
628 S12 and S13 present the ratios of initial and aged SOA yields under high and low NO<sub>x</sub>  
629 conditions. For initial SOA yields, 11 of the 56 cases are missing and 14 cases are  
630 designed to exhibit no NO<sub>x</sub> dependence, leaving 31 meaningful comparisons. Among  
631 these, 29 cases show lower SOA yields under high NO<sub>x</sub> conditions. For aged SOA  
632 yields, 5 cases are missing and 14 are designed with no NO<sub>x</sub> effect, leaving 37  
633 meaningful comparisons, of which 34 also show lower SOA yields under high NO<sub>x</sub>  
634 conditions. These results indicate a general trend of higher SOA yields under low NO<sub>x</sub>  
635 conditions, although a few exceptions are observed. In some cases, the NO<sub>x</sub> effect is  
636 reversed—that is, SOA yields are higher under high NO<sub>x</sub> conditions than under low  
637 NO<sub>x</sub> conditions. This is seen for BENZ in the CAMx SOAP2 scheme, TERP in CMAQ  
638 CRACMM, and SESQ in the GEOS-Chem Complex scheme. The NO<sub>x</sub> effect on  
639 terpene-derived SOA in CRACMM is particularly noteworthy: the model predicts an  
640 eightfold increase in SOA yields under high NO<sub>x</sub> conditions compared to low NO<sub>x</sub>.  
641 This is significant given that terpenes are key SOA precursors in many forested regions,  
642 such as the Eastern U.S., where anthropogenic NO<sub>x</sub> emissions may change due to  
643 ongoing urban development (which could increase NO<sub>x</sub> levels) or the implementation  
644 of emission control technologies (which may reduce them). Experimental studies,  
645 including those by Sarrafzadeh et al. (2016) and Wildt et al. (2014), have consistently  
646 found that terpene-derived SOA yields are higher under low NO<sub>x</sub> conditions, a result  
647 that aligns with most of the evaluated schemes but contrasts with the predictions made  
648 by CRACMM.

## 649 **5. Implications**



650 **SOA schemes implemented in CTMs are diverse, making quantitative**  
651 **comparisons inherently challenging.** CTMs employ diverse approaches to simulate  
652 SOA, from simple schemes that treat SOA as non-volatile to more complex VBS  
653 schemes that utilize multiple basis sets to represent different types of precursors.  
654 Variability in how SOA aging is treated further adds to the overall diversity across  
655 schemes. In our view, such diversity is valuable from a research perspective, given that  
656 the underlying processes driving SOA formation remain uncertain and, in many cases,  
657 poorly characterized. The variation in SOA yields across different schemes reflects the  
658 extent of these uncertainties. The differences in scheme formulation, coupled with the  
659 large numbers of parameters employed in some schemes, pose practical challenges for  
660 applying multiple schemes to standardized scenarios. Addressing these challenges may  
661 require innovative approaches. Nonetheless, comparisons under standardized  
662 conditions are essential for achieving meaningful quantitative inter-comparisons.  
663 Evaluating SOA yields under standard conditions and plotting SOA yield curves (i.e.,  
664 yield vs.  $C_{OA}$ ) are effective strategies for identifying similarities and differences among  
665 schemes. However, it is important to note that the results presented here may not fully  
666 capture the ranges of conditions encountered in three-dimensional atmospheric  
667 simulations.

668 **Initial SOA yields vary substantially across schemes and while many schemes**  
669 **consider SOA aging, the aging effects vary.** Evaluating seven precursor types under  
670 both high and low  $NO_x$  conditions yields 14 distinct comparisons. Across these  
671 comparisons, the ratio of maximum to minimum initial yields (max/min) ranges from  
672 1.8 to >1000 with a median max/min of 4.2 (Table 1). Among the eight schemes  
673 examined, three (CAMx SOAP2, GEOS-Chem schemes) do not include explicit SOA  
674 aging processes. Four schemes account for aging in a subset of precursor types and/or  
675  $NO_x$ -conditions, while only one (CMAQ CRACMM) includes aging for all precursors.  
676 Aging mechanisms considered by these schemes include gas-phase OH-oxidation of  
677 evaporated SOA, particle-phase oligomerization, hydrolysis, and photolysis. The  
678 impacts of aging on SOA yields vary by scheme and precursor (Table S14): in 67 of the



679 98 evaluated cases (defined as one scheme/precursor/NO<sub>x</sub>-condition combination,  
680 CRACMM excluded), aging has no effect; in 31 cases, it increases SOA yields.  
681 Considering the aging effects, the ratio of max/min aged yields ranges from 5.0 to > 70,  
682 with a median value of 8.3 (Table 2). The relative rankings of precursors by their  
683 initial/aged SOA yields differ across schemes (Table S15 and Table S16), indicating  
684 that different aging schemes can lead to divergent conclusions regarding the relative  
685 importance of specific SOA precursors—a consideration with potential implications for  
686 policy guidance.

687 SOA aging remains an area in need of improved representation, with careful attention  
688 required to ensure consistent underlying assumptions. Notably, only the two CAMx  
689 schemes incorporate condensed-phase SOA photolysis, despite growing evidence that  
690 both anthropogenic and biogenic SOA can undergo substantial photolytic depletion  
691 (Hodzic et al., 2016; Baboomian et al., 2020), although a portion of SOA appears  
692 recalcitrant to such degradation (O’Brien and Kroll, 2019).

693 **Large uncertainty exists for IVOC SOA yields.** The SOA yields from IVOCs show  
694 wider variation (from negligible to 1.0 g/g) than for other anthropogenic precursors  
695 (Table 1 and Table 2), partly due to different assumptions across schemes. For example,  
696 schemes such as WRF-Chem MOSAIC and CHIMERE VBS predict very low initial  
697 yields from IVOC, based on the assumption that several generations of oxidation are  
698 required before forming condensable products. Even after one day of aging, IVOC SOA  
699 yields remain highly variable, ranging from 0.02 to 1.20 g/g. Although IVOC are  
700 generally classified based on volatility, factors such as high molecular weight or the  
701 presence of polar functional groups can shift compounds into the IVOC volatility range  
702 (Pankow and Asher, 2008). As a result, volatility and SOA yield are not necessarily well  
703 correlated (Donahue et al., 2011). Improving model representations of IVOC-derived  
704 SOA yields will require more detailed differentiation of IVOC emissions into multiple  
705 subtypes, as illustrated by the CRACMM scheme (Pye et al. 2023). A unified  
706 classification or “lumping” scheme for IVOC would be particularly advantageous,  
707 allowing multiple models to utilize a common emissions framework and enabling more





708 direct comparisons of IVOC SOA yields. Improving the representation of oxygenated  
709 VOCs with reduced volatility—such as glycols and glycol ethers—within gas-phase  
710 chemical mechanisms can also support improved differentiation of IVOC-related SOA  
711 formation (Yarwood and Tuite, 2024; Yu et al., 2024). More generally, a yield-based  
712 lumping approach for IVOCs (e.g., categorizing them into low, medium, or high yield  
713 classes) may be more practical to implement than strictly chemically-based schemes.

714 **Determining experimental SOA yields also presents significant challenges.**  
715 Laboratory experiments play a crucial role in guiding SOA model development and  
716 constraining key model parameters, particularly yields. However, these experiments are  
717 subject to operational and design limitations, including the need to account for chamber  
718 wall effects (Zhang et al., 2014) and to achieve atmospherically relevant concentration  
719 ranges (Peng et al., 2022; Kenagy et al., 2024). The role of autoxidation reactions in  
720 SOA formation further complicates the design of atmospherically relevant experiments,  
721 as discussed in detail by Kenagy et al. (2024). For instance, studying a reaction  
722 mechanism that includes RO<sub>2</sub> radical autoxidation at a rate of 0.1 s<sup>-1</sup> requires that the  
723 effective rates of competing bimolecular reactions, particularly RO<sub>2</sub> + NO, be reduced  
724 to 0.1 s<sup>-1</sup> or lower. This necessitates NO mixing ratios below approximately 5 ppb,  
725 which are now typical of photochemically active urban environments such as Los  
726 Angeles (Praske et al., 2018). Many SOA chamber experiments designed to investigate  
727 high NO<sub>x</sub> conditions exceed 5 ppb NO, thereby preventing autoxidation. Some chamber  
728 experiments, such as those by Sarrafzadeh et al. (2016), have been specifically designed  
729 to achieve atmospherically relevant NO (and other radicals) concentrations, making  
730 their results particularly valuable for SOA model development. In contrast, oxidation  
731 flow reactors face greater challenges (Peng et al., 2019) than chamber experiments in  
732 studying SOA formation due to their amplification of radical concentrations, which  
733 significantly shortens RO<sub>2</sub> lifetime and effectively suppresses autoxidation reactions.  
734 Wennberg (2023) has suggested shifting from the conventional terminology of high/low  
735 NO<sub>x</sub> to high/low NO to emphasize the critical role of NO concentration in determining  
736 RO<sub>2</sub> radical fate.



## 6. Conclusions

In this study, we compared SOA formation by eight schemes implemented in five widely used CTMs. For each SOA scheme, we quantified the initial SOA mass yields under standardized conditions ( $T=298\text{ K}$  and  $C_{OA}=10\text{ }\mu\text{g/m}^3$ ), showed how the initial yield varies with  $C_{OA}$ , and quantified how one day of simulated atmospheric aging changed the initial yield. We calculated yields for 7 SOA precursor types (4 anthropogenic and 3 biogenic) under both high and low  $\text{NO}_x$  conditions.

The lack of consistency across eight current SOA schemes reviewed here reveals a lack of consensus within the air quality modelling community, notwithstanding substantial efforts to greatly expand the scientific knowledge base related to SOA formation over recent decades. Evaluating SOA schemes using ambient measurements is unlikely to produce consensus because large uncertainties in the SOA schemes are confounded with large uncertainties in precursor emission estimates. In our view, there is no objective basis for preferring one SOA scheme over another considering the high degree of uncertainty presented here. Complex SOA schemes may be valuable to research for investigating linkages between precursors and SOA, but conversely, complexity may be a hindrance to the work of air quality planning because it adds to computational burdens and makes the science more difficult to comprehend and communicate. Notably, very simple SOA schemes have performed as well or better than complex schemes in their ability to simulate ambient OA measurements when driven by ambient precursor measurements (Hodzic and Jimenez, 2011; Pai et al., 2020). Complex schemes can introduce responses to conditions, such as  $\text{NO}_x$  concentration, that may be unexpected and should be overtly evaluated if they have policy relevance, such as the  $\text{NO}_x$  effect on SOA yield from BVOC. Simple schemes with well-characterized SOA yields and responses can have an important place in air quality modelling to support decision making which includes studies that value the health-burdens of air pollution as well as traditional emissions management planning.

In addition, a majority of the eight schemes reviewed here are based on the VBS approach and we expect that sampling a larger number of model schemes would not



change this finding. VBS schemes have practical advantages because experimental studies frequently summarize their data (e.g., SOA yields, POA volatility) in a VBS frame which makes for direct translation of these data into a VBS model scheme. However, VBS data can be translated into a different frame (e.g., a two-product scheme) for SOA formation or for representing the partial evaporation of POA emissions, as illustrated by Huang et al. (2024). Therefore, scheme developers can consider using non VBS-based approaches to gain advantages of simplicity and efficiency. The findings summarized above underscore the importance of understanding the limitations of available SOA schemes when applied to air quality management and policy development. The choice of model/scheme can significantly influence the predicted SOA concentrations and their evolution over time, which in turn affects air quality forecasts, assessments and regulations.

#### **DATA AVAILABILITY**

The source data for figures are available at Zenodo (10.5281/zenodo.16757660).

#### **AUTHOR CONTRIBUTIONS**

G.Y. and L.H. designed the research. L.H. performed the data collection, yields calculation, and data analysis. L.H. and G.Y. wrote the manuscript. B. C., Z. W., K.T., and P.V. contributed to data analysis and revision of the manuscript. Y.W. and L.L. contributed to the revision of the manuscript. All authors contributed to the manuscript preparation and discussions.

#### **ACKNOWLEDGMENTS**

This work is supported by the Shanghai Technical Service Center of Science and Engineering Computing, Shanghai University. This study was financially supported by the National Natural Science Foundation of China (Grant No. 42375103, 42375102) and Electric Power Research Institute (EPRI), Palo Alto, California.

#### **COMPETING INTERESTS**

The authors declare no competing interests.

#### **REFERENCES**

Appel, K. W., Bash, J. O., Fahey, K. M., Foley, K. M., Gilliam, R. C., Hogrefe, C., Hutzell, W. T., Kang, D., Mathur, R., Murphy, B. N., Napelenok, S. L., Nolte,



- 800 C. G., Pleim, J. E., Pouliot, G. A., Pye, H. O. T., Ran, L., Roselle, S. J., Sarwar,  
801 G., Schwede, D. B., Sidi, F. I., Spero, T. L., and Wong, D. C.: The Community  
802 Multiscale Air Quality (CMAQ) model versions 5.3 and 5.3.1: system updates  
803 and evaluation, *Geosci. Model Dev.*, 14(5), 2867–2897,  
804 <https://doi.org/10.5194/gmd-14-2867-2021>, 2021.
- 805 Ahmadv, R., McKeen, S. A., Robinson, A. L., Bahreini, R., Middlebrook, A. M., de  
806 Gouw, J. A., Meagher, J., Hsie, E.-Y. , Edgerton, E., Shaw, S., and Trainer, M.:  
807 A volatility basis set model for summertime secondary organic aerosols over the  
808 eastern United States in 2006, *J. Geophys. Res.:Atmos.*, 117,  
809 <https://doi.org/10.1029/2011jd016831>, 2012.
- 810 Beekmann, M. and Vautard, R.: A modelling study of photochemical regimes over  
811 Europe: robustness and variability, *Atmos. Chem. Phys.*, 10, 10067–10084,  
812 <https://doi.org/10.5194/acp-10-10067-2010>, 2010.
- 813 Baboomian, V. J., Gu, Y., and Nizkorodov, S. A.: Photodegradation of Secondary  
814 Organic Aerosols by Long-Term Exposure to Solar Actinic Radiation, *ACS Earth*  
815 *Space Chem.*, 4, 1078–1089,  
816 <https://doi.org/10.1021/acsearthspacechem.0c00088>, 2020.
- 817 Cappa, C. D. and Wilson, K. R.: Multi-generation gas-phase oxidation, equilibrium  
818 partitioning, and the formation and evolution of secondary organic aerosol,  
819 *Atmos. Chem. Phys.*, 12, 9505–9528, <https://doi.org/10.5194/acp-12-9505-2012>,  
820 2012.
- 821 Chang, X., Zhao, B., Zheng, H., Wang, S., Cai, S., Guo, F., Gui, P., Huang, G., Wu,  
822 D., Han, L., Xing, J., Man, H., Hu, R., Liang, C., Xu, Q., Qiu, X., Ding, D., Liu,  
823 K., Han, R., and Robinson, A. L.: Full-volatility emission framework corrects  
824 missing and underestimated secondary organic aerosol sources, *One Earth.*, 5,  
825 403–412, <https://doi.org/10.1016/j.oneear.2022.03.015>, 2022.
- 826 Chen, Q., Miao, R., Geng, G., Shrivastava, M., Dao, X., Xu, B., Sun, J., Zhang, X.,  
827 Liu, M., Tang, G., Tang, Q., Hu, H., Huang, R.-J., Wang, H., Zheng, Y., Qin, Y.,  
828 Guo, S., Hu, M., and Zhu, T.: Widespread 2013–2020 decreases and reduction  
829 challenges of organic aerosol in China, *Nat. Commun.*, 15,  
830 <https://doi.org/10.1038/s41467-024-48902-0>, 2024.
- 831 CHIMERE Users Guide 2023: <https://www.lmd.polytechnique.fr/chimere/> last access:  
832 15 February 2024.
- 833 Cholakian, A., Beekmann, M., Colette, A., Coll, I., Siour, G., Sciare, J., Marchand,  
834 N., Couvidat, F., Pey, J., Gros, V., Sauvage, S., Michoud, V., Sellegri, K.,  
835 Colomb, A., Sartelet, K., DeWitt, H. L., Elser, M., Prévôt, A. S. H., Szidat, S.,  
836 and Dulac, F.: Simulation of fine organic aerosols in the western Mediterranean  
837 area during the ChArMEx 2013 summer campaign, *Atmos. Chem. Phys.*, 18,  
838 7287–7312, <https://doi.org/10.5194/acp-18-7287-2018>, 2018.



- 839 Couvidat, F., Bessagnet, B., Garcia-Vivanco, M., Real, E., Menut, L., and Colette, A.:  
840 Development of an inorganic and organic aerosol model (CHIMERE 2017  $\beta$   
841 v1.0): seasonal and spatial evaluation over Europe, *Geosci. Model Dev.*, 11, 165–  
842 194, <https://doi.org/10.5194/gmd-11-165-2018>, 2018.
- 843 Donahue, N. M., Robinson, A. L., Stanier, C. O., and Pandis, S. N.: Coupled  
844 Partitioning, Dilution, and Chemical Aging of Semivolatile Organics, *Environ.*  
845 *Sci. Technol.*, 40, 2635–2643, <https://doi.org/10.1021/es052297c>, 2006.
- 846 Donahue, N. M., Epstein, S. A., Pandis, S. N., and Robinson, A. L.: A two-  
847 dimensional volatility basis set: 1. organic-aerosol mixing thermodynamics,  
848 *Atmos. Chem. Phys.*, 11, 3303–3318, <https://doi.org/10.5194/acp-11-3303-2011>,  
849 2011.
- 850 Emery, C., Baker, K., Wilson, G. and Yarwood, G.: Comprehensive Air Quality  
851 Model with Extensions: Formulation and Evaluation for Ozone and Particulate  
852 Matter over the US. *Atmosphere*, 15(10), <https://doi.org/10.3390/atmos15101158>,  
853 2024
- 854 Honoré, C., Rouil, L., Vautard, R., Beekmann, M., Bessagnet, B., Dufour, A.,  
855 Elichegaray, C., Flaud, J.-M., Malherbe, L., Meleux, F., Menut, L., Martin, D.  
856 W., Peuch, A., Peuch, V.-H., Poisson, N.: Predictability of European air quality:  
857 Assessment of 3 years of operational forecasts and analyses by the PREV’AIR  
858 system, *J. Geophys. Res.: Atmos.*, 113, <https://doi.org/10.1029/2007jd008761>,  
859 2008.
- 860 Hodzic, A. and Jimenez, J. L.: Modeling anthropogenically controlled secondary  
861 organic aerosols in a megacity: A simplified framework for global and climate  
862 models, *Geosci. Model Dev.*, 4, 901–917, [https://doi.org/10.5194/gmd-4-901-](https://doi.org/10.5194/gmd-4-901-2011)  
863 2011, 2011.
- 864 Hodzic, A., Jimenez, J. L., Madronich, S., Aiken, A. C., Bessagnet, B., Curci, G.,  
865 Fast, J., Lamarque, J. F., Onasch, T. B., Roux, G., Ulbrich, I. M.: Modeling  
866 organic aerosols during MILAGRO: application of the CHIMERE model and  
867 importance of biogenic secondary organic aerosols, *Atmos. Chem. Phys. Discuss.*,  
868 <https://doi.org/10.5194/acpd-9-12207-2009>, 2009.
- 869 Hodzic, A., Jimenez, J. L., Madronich, S., Canagaratna, M. R., DeCarlo, P. F.,  
870 Kleinman, L., and Fast, J.: Modeling organic aerosols in a megacity: potential  
871 contribution of semi-volatile and intermediate volatility primary organic  
872 compounds to secondary organic aerosol formation, *Atmos. Chem. Phys.*, 10,  
873 5491–5514, <https://doi.org/10.5194/acp-10-5491-2010>, 2010.
- 874 Hodzic, A., Kasibhatla, P. S., Jo, D. S., Cappa, C. D., Jimenez, J. L., Madronich, S.,  
875 and Park, R. J.: Rethinking the global secondary organic aerosol (SOA) budget:  
876 Stronger production, faster removal, shorter lifetime, *Atmos. Chem. Phys.*, 16,  
877 7917–7941, <https://doi.org/10.5194/acp-16-7917-2016>, 2016.



- 878 Huang, L., Liu, H., Yarwood, G., Wilson, G., Tao, J., Han, Z., Ji, D., Wang, Y., and  
879 Li, L.: Modeling of secondary organic aerosols (SOA) based on two commonly  
880 used air quality models in China: Consistent S/IVOCs contribution but large  
881 differences in SOA aging, *Sci. Total Environ.*, 903, 166162,  
882 <https://doi.org/10.1016/j.scitotenv.2023.166162>, 2023.
- 883 Huang, L., Wu, Z., Liu, H., Yarwood, G., Huang, D., Wilson, G., Chen, H., Ji, D.,  
884 Tao, J., Han, Z., Wang, Y., Wang, H., Huang, C., and Li, L.: An improved  
885 framework for efficiently modeling organic aerosol (OA) considering primary  
886 OA evaporation and secondary OA formation from VOCs, IVOCs, and SVOCs,  
887 *Environ. Sci.: Atmos.*, 4, 1064–1078, <https://doi.org/10.1039/d4ea00060a>, 2024.
- 888 Huang, R.-J., Zhang, Y., Bozzetti, C., Ho, K.-F., Cao, J.-J., Han, Y., Daellenbach, K.  
889 R., Slowik, J. G., Platt, S. M., Canonaco, F., Zotter, P., Wolf, R., Pieber, S. M.,  
890 Bruns, E. A., Crippa, M., Ciarelli, G., Piazzalunga, A., Schwikowski, M.,  
891 Abbaszade, G., and Schnelle-Kreis, J.: High secondary aerosol contribution to  
892 particulate pollution during haze events in China, *Nature.*, 514, 218–222,  
893 <https://doi.org/10.1038/nature13774>, 2014.
- 894 Koo, B., Knipping, E., and Yarwood, G.: 1.5-Dimensional volatility basis set  
895 approach for modeling organic aerosol in CAMx and CMAQ, *Atmos. Environ.*,  
896 95, 158–164, <https://doi.org/10.1016/j.atmosenv.2014.06.031>, 2014.
- 897 Lane, T. E., Donahue, N. M., and Pandis, S. N.: Simulating secondary organic aerosol  
898 formation using the volatility basis-set approach in a chemical transport model,  
899 *Atmos. Environ.*, 42, 7439–7451, <https://doi.org/10.1016/j.atmosenv.2008.06.026>,  
900 2008.
- 901 Li, J., Zhang, H., Li, L., Ye, F., Wang, H., Guo, S., Zhang, N., Qin, M., and Hu, J.:  
902 Modeling Secondary Organic Aerosols in China: State of the Art and  
903 Perspectives, *Curr. Pollut. Rep.*, 9(1), 22–45, [https://doi.org/10.1007/s40726-022-](https://doi.org/10.1007/s40726-022-00246-3)  
904 00246-3, 2023.
- 905 Luecken, D. J., Phillips, S., Sarwar, G., and Jang, C.: Effects of using the CB05 vs.  
906 SAPRC99 vs. CB4 chemical mechanism on model predictions: Ozone and gas-  
907 phase photochemical precursor concentrations, *Atmos. Environ.*, 42, 5805–  
908 5820, <https://doi.org/10.1016/j.atmosenv.2007.08.056>, 2008.
- 909 Ma, S., Zhang, X., Gao, C., Tong, Q., Xiu, A., Zhao, H., and Zhang, S.: Simulating  
910 Performance of CHIMERE on a Late Autumnal Dust Storm over Northern China,  
911 *Sustainability.*, 11, 1074, <https://doi.org/10.3390/su11041074>, 2019.
- 912 Ma, P. K., Zhao, Y., Robinson, A. L., Worton, D. R., Goldstein, A. H., Ortega, A. M.,  
913 Jimenez, J. L., Zotter, P., Prévôt, A. S. H., Szidat, S., and Hayes, P. L.:  
914 Evaluating the impact of new observational constraints on P-S/IVOC emissions,  
915 multi-generation oxidation, and chamber wall losses on SOA modeling for Los  
916 Angeles, CA, *Atmos. Chem. Phys.*, 17, 9237–9259,  
917 <https://doi.org/10.5194/acp-17-9237-2017>, 2017.



- 918 Marais, E. A., Jacob, D. J., Jimenez, J. L., Campuzano-Jost, P., Day, D. A., Hu, W.,  
919 Krechmer, J. E., Zhu, L., Kim, P. K., Miller, C. J., Fisher, J. A., Travis, K. R., Yu,  
920 K., Hanisco, T. F., Wolfe, G. M., Arkinson, H. L., Pye, H. O. T., Froyd, K. D.,  
921 Liao, J., and McNeill, V., Faye,,: Aqueous-phase mechanism for secondary organic  
922 aerosol formation from isoprene: application to the southeast United States and  
923 co-benefit of SO<sub>2</sub> emission controls, *Atmos. Chem. Phys.*, 16, 1603–1618,  
924 <https://doi.org/10.5194/acp-16-1603-2016>, 2016.
- 925 Murphy, B. N., Sonntag, D., Seltzer, K. M., Pye, H. O. T., Allen, C., Murray, E.,  
926 Toro, C., Gentner, D. R., Huang, C., Shantanu Jathar, Li, L., May, A. A., and  
927 Robinson, A. L.: Reactive organic carbon air emissions from mobile sources in  
928 the United States, *Atmos. Chem. Phys.*, 23, 13469–13483,  
929 <https://doi.org/10.5194/acp-23-13469-2023>, 2023.
- 930 Murphy, B. N., Woody, M., Jimenez, J. L., Carlton, A. G., Hayes, P. M., Liu, S., Ng,  
931 N. L., Russell, L., Ari Setyan, Xu, L., Young, J. F., Zaveri, R. A., Zhang, Q., and  
932 Pye, H. O. T.: Semivolatile POA and parameterized total combustion SOA in  
933 CMAQv5.2: impacts on source strength and partitioning, *Atmos. Chem. Phys.*, 17,  
934 11107–11133, <https://doi.org/10.5194/acp-17-11107-2017>, 2017.
- 935 Murphy, B., Appel, W., Bash, J., Fahey, K., Henderson, B., Hutzell, B., Kang, D.,  
936 Luecken, D., Mathur, R., Napelenok, S., Nolte, C., Pye, H. O. T., Pleim, J., Qin,  
937 M., Ran, L., Roselle, S., Sarwar, G., Schwede, D., Shu, Q., Spero, T., 2018:  
938 Scientific and Structural Developments in CMAQv5.3. 2018 CMAS Conference,  
939 Chapel Hill, North Carolina, 22–24 October 2018.
- 940 Nault, B. A., Jo, D. S., McDonald, B. C., Campuzano-Jost, P., Day, D. A., Hu, W.,  
941 Schroder, J. C., Allan, J., Blake, D. R., Canagaratna, M. R., Coe, H., Coggon, M.  
942 M., DeCarlo, P. F., Diskin, G. S., Dunmore, R., Flocke, F., Fried, A., Gilman, J.  
943 B., Gkatzelis, G., Hamilton, J. F., Hanisco, T. F., Hayes, P. L., Henze, D. K.,  
944 Hodzic, A., Hopkins, J., Hu, M., Huey, L. G., Jobson, B. T., Kuster, W. C.,  
945 Lewis, A., Li, M., Liao, J., Nawaz, M. O., Pollack, I. B., Peischl, J., Rappenglück,  
946 B., Reeves, C. E., Richter, D., Roberts, J. M., Ryerson, T. B., Shao, M.,  
947 Sommers, J. M., Walega, J., Warneke, C., Weibring, P., Wolfe, G. M., Young, D.  
948 E., Yuan, B., Zhang, Q., de Gouw, J. A., and Jimenez, J. L.: Secondary organic  
949 aerosols from anthropogenic volatile organic compounds contribute substantially  
950 to air pollution mortality, *Atmos. Chem. Phys.*, 21, 11201–11224,  
951 <https://doi.org/10.5194/acp-21-11201-2021>, 2021.
- 952 O'Brien, R. E. and Kroll, J. H.: Photolytic Aging of Secondary Organic Aerosol:  
953 Evidence for a Substantial Photo-Recalcitrant Fraction, *J. Phys. Chem. Lett.*, 10,  
954 4003–4009, <https://doi.org/10.1021/acs.jpclett.9b01417>, 2019.
- 955 Pankow, J. F. and Asher, W. E.: SIMPOL.1: a simple group contribution method for  
956 predicting vapor pressures and enthalpies of vaporization of multifunctional  
957 organic compounds, *Atmos. Chem. Phys.*, 8, 2773–2796,  
958 <https://doi.org/10.5194/acp-8-2773-2008>, 2008.





- 959   Pai, S. J., Heald, C. L., Pierce, J. R., Farina, S. C., Marais, E. A., Jimenez, J. L.,  
960       Campuzano-Jost, P., Nault, B. A., Middlebrook, A. M., Coe, H., Shilling, J. E.,  
961       Bahreini, R., Dingle, J. H., and Vu, K.: An evaluation of global organic aerosol  
962       schemes using airborne observations, *Atmos. Chem. Phys.*, 20, 2637–2665,  
963       <https://doi.org/10.5194/acp-20-2637-2020>, 2020.
- 964   Murphy, B. N. and Pandis, S. N.: Simulating the Formation of Semivolatile Primary  
965       and Secondary Organic Aerosol in a Regional Chemical Transport Model,  
966       *Environ. Sci. Technol.*, 43, 4722–4728, <https://doi.org/10.1021/es803168a>, 2009.
- 967   Pankow, J. F.: An absorption model of the gas/aerosol partitioning involved in the  
968       formation of secondary organic aerosol, *Atmos. Environ.*, 28, 189–193,  
969       [https://doi.org/10.1016/1352-2310\(94\)90094-9](https://doi.org/10.1016/1352-2310(94)90094-9), 1994.
- 970   Pennington, E. A., Seltzer, K. M., Murphy, B. N., Qin, M., Seinfeld, J. H., and Pye,  
971       H. O. T.: Modeling secondary organic aerosol formation from volatile chemical  
972       products, *Atmos. Chem. Phys.*, 21, 18247–18261, [https://doi.org/10.5194/acp-](https://doi.org/10.5194/acp-21-18247-2021)  
973       21-18247-2021, 2021.
- 974   Pennington, E. A., Wang, Y., Schulze, B. C., Seltzer, K. M., Yang, J., Zhao, B., Jiang,  
975       Z., Shi, H., Venecek, M., Chau, D., Murphy, B. N., Kenseth, C. M., Ward, R. X.,  
976       Pye, H. O. T., and Seinfeld, J. H.: An updated modeling framework to simulate  
977       Los Angeles air quality – Part 1: Model development, evaluation, and source  
978       apportionment, *Atmos. Chem. Phys.*, 24, 2345–2363,  
979       <https://doi.org/10.5194/acp-24-2345-2024>, 2024.
- 980   Pye, H. O. T., Chan, A. W. H., Barkley, M. P., and Seinfeld, J. H.: Global modeling  
981       of organic aerosol: the importance of reactive nitrogen ( $\text{NO}_x$  and  $\text{NO}_3$ ), *Atmos.*  
982       *Chem. Phys.*, 10, 11261–11276, <https://doi.org/10.5194/acp-10-11261-2010>,  
983       2010.
- 984   Pye, H. O. T., Pinder, R. W., Piletic, I. R., Xie, Y., Capps, S. L., Lin, Y.-H., Surratt, J.  
985       D., Zhang, Z., Gold, A., Luecken, D. J., Hutzell, W. T., Jaoui, M., Offenberg, J.  
986       H., Kleindienst, T. E., Lewandowski, M., Edney, E. O.: Epoxide Pathways  
987       Improve Model Predictions of Isoprene Markers and Reveal Key Role of Acidity  
988       in Aerosol Formation, *Environ. Sci. Technol.*, 47, 11056–11064,  
989       <https://doi.org/10.1021/es402106h>, 2013.
- 990   Pye, H. O. T., D’Ambro, E. L., Lee, B. H., Schobesberger, S., Takeuchi, M., Zhao, Y.,  
991       Lopez-Hilfiker, F., Liu, J., Shilling, J. E., Xing, J., Mathur, R., Middlebrook, A.  
992       M., Liao, J., Welti, A., Graus, M., Warneke, C., de Gouw, J. A., Holloway, J. S.,  
993       Ryerson, T. B., Pollack, I. B., Thornton, J. A.: Anthropogenic enhancements to  
994       production of highly oxygenated molecules from autoxidation, *Proc. Natl.*  
995       *Acad. Sci.*, 116, 6641–6646, <https://doi.org/10.1073/pnas.1810774116>, 2019.
- 996   Pye, H. O. T., Cavin Ward-Caviness, Murphy, B., K. Wyat Appel, and Seltzer, K. M.:  
997       Secondary organic aerosol association with cardiorespiratory disease mortality in





- 998 the United States, *Nat. Commun.*, 12, [https://doi.org/10.1038/s41467-021-27484-](https://doi.org/10.1038/s41467-021-27484-1)  
999 1, 2021.
- 1000 Pye, H. O. T., Place, B. K., Murphy, B. N., Seltzer, K. M., D'Ambro, E. L., Allen, C.,  
1001 Piletic, I. R., Farrell, S., Schwantes, R. H., Coggon, M. M., Saunders, E., Xu, L.,  
1002 Sarwar, G., Hutzell, W. T., Foley, K. M., Pouliot, G., Bash, J., and Stockwell, W.  
1003 R.: Linking gas, particulate, and toxic endpoints to air emissions in the  
1004 Community Regional Atmospheric Chemistry Multiphase Mechanism  
1005 (CRACMM), *Atmos. Chem. Phys.*, 23, 5043–5099, [https://doi.org/10.5194/acp-](https://doi.org/10.5194/acp-23-5043-2023)  
1006 23-5043-2023, 2023.
- 1007 Ramboll, 2022: CAMx User's Guide, Version 7.20.  
1008 <https://www.camx.com/download/source/> last access: 15 February 2024.
- 1009 Robinson, A. L., Donahue, N. M., Shrivastava, M. K., Weitkamp, E. A., Sage, A. M.,  
1010 Grieshop, A. P., Lane, T. E., Pierce, J. R., and Pandis, S. N.: Rethinking Organic  
1011 Aerosols: Semivolatile Emissions and Photochemical Aging, *Science.*, 315,  
1012 1259–1262, <https://doi.org/10.1126/science.1133061>, 2007.
- 1013 Sarrafzadeh, M., Wildt, J., Iida Pullinen, Springer, M., Kleist, E., Tillmann, R.,  
1014 Schmitt, S. H., Wu, C., Mentel, T. F., Zhao, D., Hastie, D. R., and Kiendler-  
1015 Scharr, A.: Impact of NO<sub>x</sub> and OH on secondary organic aerosol formation from  
1016  $\beta$ -pinene photooxidation, *Atmos. Chem. Phys.*, 16, 11237–11248,  
1017 <https://doi.org/10.5194/acp-16-11237-2016>, 2016.
- 1018 Sasidharan, S., He, Y., Akherati, A., Qi, L., Li, W., Cocker, D. R., McDonald, B.,  
1019 Coggon, M. M., Seltzer, K. M., Pye, T., Pierce, J. R., and Jathar, S. H.: Secondary  
1020 Organic Aerosol Formation from Volatile Chemical Product Emissions: Model  
1021 Parameters and Contributions to Anthropogenic Aerosol, *Environ. Sci. Technol.*,  
1022 57, 11891–11902, <https://doi.org/10.1021/acs.est.3c00683>, 2023.
- 1023 Sciare, J., d'Argouges, O., Zhang, Q. J., Sarda-Estève, R., Gaimoz, C., Gros, V.,  
1024 Beekmann, M., and Sanchez, O.: Comparison between simulated and observed  
1025 chemical composition of fine aerosols in Paris (France) during springtime:  
1026 contribution of regional versus continental emissions, *Atmos. Chem. Phys.*, 10,  
1027 11987–12004, <https://doi.org/10.5194/acp-10-11987-2010>, 2010.
- 1028 Schell, B., Ackermann, I. J., Hass, H., Binkowski, F. S., and Ebel, A.: Modeling the  
1029 formation of secondary organic aerosol within a comprehensive air quality model  
1030 system, *J. Geophys. Res.:Atmos.*, 106, 28275–28293,  
1031 <https://doi.org/10.1029/2001jd000384>, 2001.
- 1032 Shrivastava, M., Easter, R. C., Liu, X., Zelenyuk, A., Singh, B., Zhang, K., Ma, P.,  
1033 Chand, D., Ghan, S. J., Jimenez, J. L., Zhang, Q., Fast, J. D., Rasch, P. J., and  
1034 Tiitta, P.: Global transformation and fate of SOA: Implications of low-volatility  
1035 SOA and gas-phase fragmentation reactions, *J. Geophys. Res.:Atmos.*, 120, 4169–  
1036 4195, <https://doi.org/10.1002/2014jd022563>, 2015.



- 1037 Shrivastava, M. B., Fast, J. D., Easter, R. C., Gustafson, W. I., Zaveri, R. A., Jimenez,  
1038 J. L., Saide, P. E., and Hodzic, A.: Modeling organic aerosols in a megacity:  
1039 comparison of simple and complex representations of the volatility basis set  
1040 approach, *Atmos. Chem. Phys.*, 11, 6639–6662, [https://doi.org/10.5194/acp-11-](https://doi.org/10.5194/acp-11-6639-2011)  
1041 6639-2011, 2011.
- 1042 Strader, R. Lurmann, F., and Pandis, S. N.: Evaluation of secondary organic aerosol  
1043 formation in winter, *Atmos. Environ.*, 33, 4849–4863,  
1044 [https://doi.org/10.1016/s1352-2310\(99\)00310-6](https://doi.org/10.1016/s1352-2310(99)00310-6), 1999.
- 1045 Tsimpidi, A. P., Karydis, V. A., Pandis, S. N., and Lelieveld, J.: Global combustion  
1046 sources of organic aerosols: model comparison with 84 AMS factor-analysis data  
1047 sets, *Atmos. Chem. Phys.*, 16, 8939–8962, [https://doi.org/10.5194/acp-16-8939-](https://doi.org/10.5194/acp-16-8939-2016)  
1048 2016, 2016.
- 1049 Vitali, B., Bettineschi, M., Cholakian, A., Zardi, D., Bianchi, F., Sinclair, V. A.,  
1050 Mikkola, J., Paolo Cristofanelli, Marinoni, A., Mazzini, M., Heikkinen, L.,  
1051 Aurela, M., Paglione, M., Bertrand Bessagnet, Paolo Tuccella, and Ciarelli, G.:  
1052 Analysis of chemical and transport processes of biogenic aerosols over the  
1053 northern Apennines: insights from the WRF-CHIMERE model, *Environ. Sci.: Atmos.*, 4, 967–987, <https://doi.org/10.1039/d4ea00040d>, 2024.
- 1055 Wildt, J., Mentel, T. F., Kiendler-Scharr, A., Hoffmann, T., Andres, S., Ehn, M.,  
1056 Kleist, E., P. Müsgen, Rohrer, F., Rudich, Y., Springer, M., Tillmann, R., and  
1057 Wahner, A.: Suppression of new particle formation from monoterpene oxidation  
1058 by NO<sub>x</sub> *Atmos. Chem. Phys.*, 14, 2789–2804, [https://doi.org/10.5194/acp-14-](https://doi.org/10.5194/acp-14-2789-2014)  
1059 2789-2014, 2014.
- 1060 WRF-Chem version 4.4 Users Guide, 2022: [https://ruc.noaa.gov/wrf/wrf-](https://ruc.noaa.gov/wrf/wrf-chem/Users_guide.pdf)  
1061 chem/Users\_guide.pdf last access: 15 February 2024.
- 1062 Xu, L., Guo, H., Boyd, C. M., Klein, M., Bougiatioti, A., Cerully, K. M., Hite, J. R.,  
1063 Isaacman-VanWertz, G., Kreisberg, N. M., Knote, C., Olson, K., Koss, A.,  
1064 Goldstein, A. H., Hering, S. V., de Gouw, J., Baumann, K., Lee, S.-H., Nenes, A.,  
1065 Weber, R. J., and Ng, N. L.: Effects of anthropogenic emissions on aerosol  
1066 formation from isoprene and monoterpenes in the southeastern United States,  
1067 *Proc. Natl. Acad. Sci.*, 112, 37–42, <https://doi.org/10.1073/pnas.1417609112>,  
1068 2014.
- 1069 Yarwood, G. and Tuite, K.: Representing Ozone Formation from Volatile Chemical  
1070 Products (VCP) in Carbon Bond (CB) Chemical Mechanisms, *Atmosphere.*, 15,  
1071 178, <https://doi.org/10.3390/atmos15020178>, 2024.
- 1072 Yu, H., Møller, K. H., Buenconsejo, R. S., Crounse, J. D., Kjaergaard, H. G., and  
1073 Wennberg, P. O.: Atmospheric Photo-Oxidation of 2-Ethoxyethanol:  
1074 Autoxidation Chemistry of Glycol Ethers, *J. Phys. Chem. A.*, 127, 9564–9579,  
1075 <https://doi.org/10.1021/acs.jpca.3c04456>, 2023.



- 1076 Zawadowicz, M. A., Lee, B. H., Shrivastava, M., Zelenyuk, A., Zaveri, R. A., Flynn,  
1077 C., Thornton, J. A., and Shilling, J. E.: Photolysis Controls Atmospheric Budgets  
1078 of Biogenic Secondary Organic Aerosol, *Environ. Sci. Technol.*, 54, 3861–3870,  
1079 <https://doi.org/10.1021/acs.est.9b07051>, 2020.
- 1080 Zhang, Q., Laurent, B., Velay-Lasry, F., Ngo, R., Derognat, C., Marticorena, B., and  
1081 Albergel, A.: An air quality forecasting system in Beijing - Application to the  
1082 study of dust storm events in China in May 2008, *J. Environ. Sci.*, 24, 102–111,  
1083 [https://doi.org/10.1016/s1001-0742\(11\)60733-x](https://doi.org/10.1016/s1001-0742(11)60733-x), 2012.
- 1084 Zhang, Q. J., Beekmann, M., Drewnick, F., Freutel, F., Schneider, J., Crippa, M.,  
1085 Prevot, A. S. H., Baltensperger, U., Poulain, L., Wiedensohler, A., Sciare, J.,  
1086 Gros, V., Borbon, A., Colomb, A., Michoud, V., Doussin, J.-F., Denier van der  
1087 Gon, H. A. C., Haeffelin, M., Dupont, J.-C., Siour, G., Petetin, H., Bessagnet, B.,  
1088 Pandis, S. N., Hodzic, A., Sanchez, O., Honoré, C., and Perrussel, O.: Formation  
1089 of organic aerosol in the Paris region during the MEGAPOLI summer campaign:  
1090 evaluation of the volatility-basis-set approach within the CHIMERE model,  
1091 *Atmos. Chem. Phys.*, 13, 5767–5790, <https://doi.org/10.5194/acp-13-5767-2013>,  
1092 2013.
- 1093 Zhao, Y., Hennigan, C. J., May, A. A., Tkacik, D. S., de Gouw, J. A., Gilman, J. B.,  
1094 Kuster, W. C., Borbon, A., and Robinson, A. L.: Intermediate-Volatility Organic  
1095 Compounds: A Large Source of Secondary Organic Aerosol, *Environ. Sci.*  
1096 *Technol.*, 48, 13743–13750, <https://doi.org/10.1021/es5035188>, 2014.